SIMULATION OF ATMOSPHERIC BOUNDARY LAYER IN N.W.T.F.

By

Kapil Varshney

DEPARTMENT OF AEROSPACE ENGINEERING

Indian Institute of Technology Kanpur

APRIL, 2002

SIMULATION OF ATMOSPHERIC BOUNDARY LAYER IN N.W.T.F.

A Thesis Submitted
In Partial Fulfilment of the Requirements
for the Degree of
Master of Technology

by

KAPIL VARSHNEY

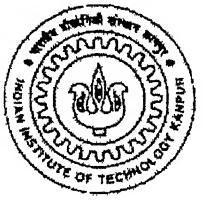

to the

DEPARTMENT OF AEROSPACE ENGINEERING
INDIAN INSTITUTE OF TECHNOLOGY KANPUR
INDIA

April, 2002

CERTIFICATE

It is certified that the work contained in the thesis entitled "***Simulation of Atmospheric Boundary Layer in N.W.T.F.***", by ***Mr. Kapil Varshney*** , has been carried out under our supervision and that this work has not been submitted elsewhere for a degree.

Dr. Vijay Gupta
Professor
Dept. of Aerospace Engineering
I.I.T Kanpur

April, 2002

To whom I indebted the most, my family: my parents; my brothers Sandeep and Avnish; and to my beloved grandparents.

Acknowledgements

I would like to thank my advisor Dr. Vijay Gupta, without his help and constructive comments this work would not have materialized. I thank him for his teaching, his guidance and his reassurance and encouragement. Being his graduate student gave me the opportunity of experiencing hard work. For this, I deeply thank him. My thanks extend to Dr.Kamal Poddar whose experience, hard work and help are greatly acknowledged. His scientific approach, strong comments and constructive ideas have left a positive impact on this work. I also extend my great gratitude to Dr. T. Gangadharaiah who taught me fluid mechanics and who never stopped clarifying and explaining many stumbling points in turbulence. Thanks are also extended to Dr. Rajeev Gupta, for his advice throughout my course work and his outstanding teaching.

I would like to also thank Shri S.S. Chauhan, Shri Chaturi Singh, Shri S.S. Sachan, Shri Suresh and Shri K. Mohan for their invaluable help.

Lastly I am thankful to my friends Om Prakash Saresta, Ankur Gupta, Pankaj Jha and Mrinal Kaushik for their constant encouragement throughout my thesis work.

Kapil Varshney

Abstract

In the present investigation we aimed at simulation of atmospheric boundary layer in National Wind Tunnel Facility (N.W.T.F.). Eighteen different configurations of passive devices like spires, barriers and slots in the test-section extended into the contraction cone have been used. Mean velocity, longitudinal turbulence intensity and integral length scales of streamwise turbulence component have been measured. The aim is to reproduce the atmospheric boundary-layer and to determine the appropriate length scale factor for modelling which will ensure correct aeroelastic behavior of structural models and the dispersion behavior in the non-aerodynamic application.

Contents

List of Figures

List of Tables

Chapter 1

Introduction

Prediction of wind loads on low-rise and high-rise structures is important to minimize human and economic losses caused by severe storms, hurricanes, tornadoes, etc. The estimated annual losses world-wide due to wind events exceed five billion dollars. As more people move into hurricane prom coastal areas, one would expect these losses to increase significantly. To a large measure, the prediction of wind loads, etc., on structures is based on tests in the wind tunnels. One of the principle problems in aeroelastic studies for the wind-prone structures is that the length of most wind-tunnel section is insufficient for the natural development of boundary layer adequately.

Atmospheric boundary-layer flows near the earth's surface are characterized by conditions which are generally not available to wind tunnels. Non-uniform boundary conditions, non-stationarities, as well as variable atmospheric and thermal conditions usually encountered in practical situations make accurate prediction of the atmospheric boundary-layer flows extremely difficult.

The depth of the atmospheric boundary layer ranges from a few centimeters up to 600 m, depending upon the wind intensity, roughness of terrain, and the angle of latitude. The thickness of the boundary layer tends to be larger as we approach the equator. Within the boundary layer, the wind speed varies from zero at the ground to the geostrophic value Ug with the elevation; its magnitude at the top of the boundary layer. Outside the boundary layer, the wind in free aymosphere flows approximately with the geostrophic speed along the isobars.

Atmospheric boundary layer is the layer where the important forces are Coriolis force, pressure gradient force, viscous stresses and Reynolds stresses.

The wind speeds are considerably lower than the speed of sound; hence incomprehensibility may be assumed in the study of the dynamics of flow.

The flow structure of the atmospheric boundary layer is complex. However, it is established that large-scale flow structures are present within the atmospheric boundary layer, i.e., large eddies exist whose orientation is a function of the shear in the mean flow and whose degree of rotation is relatively slow. The size of these eddies is also a function of the

roughness of the terrain.

The simulation of the velocity profile of the atmospheric boundary layer is relatively simple. Grids, barriers and spires have all been used to produce the desired profiles. But it is not the velocity profile alone that needs to be simulated for accurate prediction of wind-induced loads and aero-elasticity in structures. The level of turbulence and the scale of turbulence also must be simulated accurately if the experimental prediction of structural behavior is to be reliable.

The first step we can use to predict wind loads is simulation of the turbulence characteristics of the atmospheric boundary-layer. These characteristics are usually given in terms of mean flow and the turbulence parameters. Yet, one of the most important characteristics of the atmospheric surface-layer is the level of variations in such parameters. There is no question that one of the most important parameters to be simulated in relation to wind loads on structures is the Reynolds number which is based on mean velocity and on the characteristic building dimension. But, due to geometric limitations and power requirements, it is almost impossible to simulate the Reynolds number in a wind tunnel. Since the simulation of mean flow Reynolds number is not possible; it causes many problems related to simulating the turbulence characteristics. The turbulence characteristics are usually represented in terms of statistical and spectral parameters. These parameters include turbulence intensities, and integral length scales.

Based on several studies, one can conclude the following as far as predictions of pressure loads on low-rise structures: *when the wind tunnel simulation is well matched in terms of mean flow properties and longitudinal turbulence intensity, mean pressures compare reasonably well in most cases.* On the other hand, large variations exist when comparing extreme negative pressure coefficients from wind tunnel experiments with those observed in full-scale measurements. Recent studies [1] on turbulence, suggest that the simulation of lateral turbulence intensity is also important in terms of prediction of peak pressure events. One important variable that is not well represented in the parameters used for wind tunnel simulation of atmospheric turbulence are its time-varying characteristics. Parameters such as turbulence intensities, integral scales, aerodynamic roughness, and spectra are all averaged over long periods of time. As a result, important information on the time varying characteristics is not well represented in such parameters.

In this work, we use the analysis and parameters proposed by Henry W. Tieleman [2] to determine how the characteristics of the atmosphere can be simulated in a wind tunnel. The wind tunnel used in National Wind Tunnel Facility, located at Indian Institute of Technology Kanpur, is basically a very low-turbulence level tunnel, designed primarily for the development work for transport aircrafts. However, non-aeronautical application has been defined as a secondary use. The tunnel, as such, cannot be used for non-aeronautical work and the simulation of lower atmospheric winds, unless the test section is modified

with various spires, barriers, slots, roughness elements, etc. This work provides effective and reliable parameters to compare turbulence generated in the wind tunnel with that obtained in full-scale experiments. This may help to find the best wind-tunnel configuration to simulate atmospheric boundary layer within the wind tunnel.

Chapter 2

Characteristics of Atmospheric Boundary-Layers

2.1 Introduction

The natural wind environment varies so drastically with location and time that it is very difficult to define the characteristics of atmospheric boundary-layer that can be taken as the prototype.

Two of the most commonly referenced reviews of such data are presented by E.S.D.U [3-4] and Counihan [5]. The E.S.D.U data have been collated and only the final design data are presented graphically in a parametric form. Counihan on the other hand, presents and discuss the experimental data of various researchers pointing out various discrepancies, but does not prescribe a design data. E.S.D.U data is most commonly used as the prototype data in industry. Some characteristics of atmospheric boundary layer, which define the structure of prototype boundary layer, are described here.

2.2 The Boundary Layer Height

Many authors have proposed empirical formulae for predicting the height of atmospheric boundary layer. Davenport et.al. [6] suggested that boundary layer height is function of terrain type and proposed the standard heights as given in Table 2.1.

His results are fairly matched with previously published data. A boundary-layer height for rural terrain was suggested as around 300 m by many previous meteorological data.

Terrain	$\delta(m)$
Rural	274
Urban	518

Table 2.1: Boundary layer thickness for different terrains

It was represented by Counihan [5] that if the atmospheric and flat plate boundary layer data are compared on the basis of non dimensional height z/δ with $\delta = 300$ m, very little agreement is obtain for rural data. Using $\delta = 600$ m gives better agreement. Pasquill [7] suggested that the mechanical production of energy tended to approach zero at a height of 600 m, and therefore, 600 m is taken as the upper limit of boundary-layer length.

Blackadar (1967) (as quoted by Counihan [5]) suggested that the boundary-layer height is affected very little by changes in terrain roughness and this is further supported by recent studies and assumes a mean boundary-layer height of 500 m.

In choosing what may be considered as a practical and typical boundary-layer height, some compromises must be made, e.g. the boundary layer height is clearly a function of both gradient wind speed and surface roughness. On the basis of review data for high wind speeds ($U_{10} >$ 5-7 m/s) which produce adiabatic conditions, a value of 600 m is recommended by E.S.D.U. [3-4] as well as Counihan [5] as representing the average height of both rural and urban boundary-layers.

2.3 Height of the Constant Shear Stress Layer

In the constant shear-stress region, the mean wind profile follows a log-law. In most of the work done before 1972, the typical value of the thickness of the constant shear-stress layer was estimated to be around 30-50 m. Later, some authors presented as much as 200 m as its estimate. This probably was driven by the desire to extend the mathematical amenable log-law region to greater heights. But the currently accepted value of the constant shear-stress layer is 100 m as recommended by E.S.D.U. [3-4] and Counihan [5]. In this work we use this value.

2.4 Velocity Profile

The lower part of the mean velocity profiles can best be represented by a log-law. By utilizing the flat-plate boundary-layer theory of Prandtl and Von Karman, the velocity profiles can be represented in the form

$$\frac{U}{u^*} = \frac{1}{k} ln \left(\frac{z}{z_0} \right) \tag{2.1}$$

where $u*$ is the shear velocity and z_0 is the roughness length. However, Swerdrup pointed out (as quoted by Counihan [5]), that a power-law in the form

$$\frac{U}{U_R} = \left(\frac{z}{z_R} \right)^{1/\alpha} \tag{2.2}$$

provides an equally good fit to most of the meteorological data, particularly in the case of high winds. Since the power-law can be mathematically manipulated more easily than a

Terrain	Roughness Length (m)
Rural	0.01 - 0.15
Suburban	1.0
Urban	2.0 - 4.0

Table 2.2: Typical values of Roughness Length

log-law, it tends to be used more often in meteorological problems. Here $1/\alpha$ can be taken as an indication of the amount of turbulence present. The value of power index for rural terrain is proposed as 0.143 by almost all authors.

However, the recent trend is to use log-law representation for the lower 50 m. It is quite incorrect to deduce the power-law index from the measurements at this height range. However, it has been shown by many authors that power-law can be used to represent the meteorological data over a much larger height and therefore, it appears to be a more uniformly adopted procedure these days. The power-law index is, however, based on measurement outside the first 50 m range.

For rural terrain the typical value of power index used is 0.143, but for urban terrain mean-velocity measurement is much more difficult. The value of power-index for urban terrain presented by many investigators has a significant range starting from 0.23 to 0.40. This is because of different roughness of different terrain. In his investigation Davenport et.al. [6] concluded that the value of power-index that can be used are 0.28 and 0.40 for suburban and urban terrains, respectively. The data presented in E.S.D.U. [4] suggests its value 0.35 for urban terrain.

2.5 The Roughness Length

The roughness length z_0, is related to the average measure of the roughness elements of the terrain and can be obtained by fitting the log-law to the measured velocity profile.

$$\frac{U}{u^*} = \frac{1}{k} ln \left(\frac{z}{z_0} \right) \tag{2.3}$$

There is sufficient data available to deduce the typical values of roughness length in various terrains. Many authors have represented widely differing values of z_0 for various terrains. There is some indication that the roughness length depends upon the distribution of the roughness elements, and the direction of the wind should also be taken into account. The typical values of the roughness length are taken from Table 2.2.

Counihan [5] has also proposed a graph (Fig. 2.1) of the roughness length with the variation of the power index. Most of the known available data is presented in this graph. Four terrain types on the roughness length scale are indicated as:

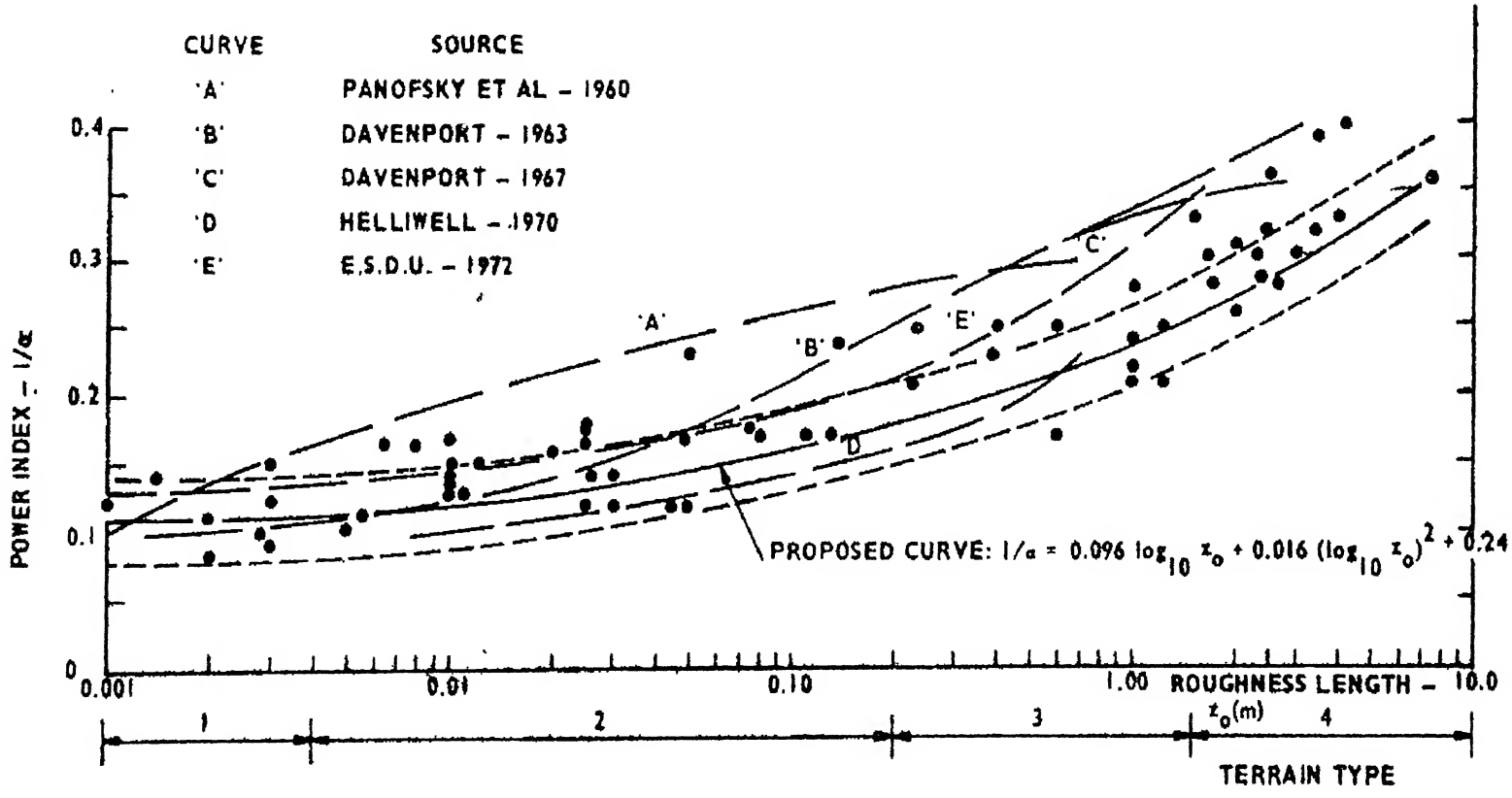

Fig. 2.1 Variation of roughness length with power index

(From Counihan [5])

1. Smooth : Ice, mud, snow,sea
2. Moderately Rough : Short grass, grass/crops, rural
3. Rough : Rural/woods, woods, suburban
4. Very Rough : Urban

The graph in Fig. 1 clearly shows that the value of power index increases with the increase of roughness length. This is to be expected, since this data will be subjected to, in addition to other errors, errors arising from insufficient fetch being available for equilibrium flow to be established. The proposed variation of the power index with the roughness length is not a mean curve through the data but has been offset downwards since most of the sources of error tend to produce over-estimates of the power index. The amount of offset was partially based on that data which was considered to be the most accurate and reliable. Clearly, an analysis of this type is subjective to some extent. In general, it can be concluded that for roughness lengths greater than 0.10 m, the curves suggested by other authors lie outside the upper scatter band of the data and are, therefore, not considered to be satisfactory. The variation of the power index with the roughness length suggested here is considered to be the most reliable.

2.6 Turbulence Intensity

The rate of production of turbulence and its intensity is a function of the Reynolds stresses and the mean-velocity profile of the flow being considered. From the earliest investigations made on atmospheric boundary layer, it was seen that turbulence levels are a function of both surface roughness and the height above the ground level. It was determined that the ratios of the three components of turbulence in atmosphere were in the ratio

$$\sqrt{\overline{u^2}} : \sqrt{\overline{v^2}} : \sqrt{\overline{w^2}} = 1.0 : 0.73 : 0.46 \tag{2.4}$$

where u, v and w are the velocity fluctuations of longitudinal, lateral and vertical velocity components of the wind. These compare very well with the ratios measured in boundary layers over a flat plate, where the ratios are, respectively, 1.0 : 0.75 : 0.54. These ratios applied from above the ground level to a height of 20 m.

For suburban and urban areas, the earlier value of longitudinal turbulence intensity ($\sqrt{\overline{u^2}}/U$) was determined to be in the range of 0.20 to 0.30. Later, this range was modified to 0.20 to 0.35. The value of longitudinal turbulence intensity depends upon the roughness of terrain and increases with the roughness of terrain. The values of both longitudinal turbulence intensity and lateral turbulence intensity increase with height up to 100 m, and then decrease above this height. Vertical component of turbulence intensity also increases

with height up to about 370 m. It is assumed that the turbulence is isotopic at and above this height for short wavelengths.

Counihan [5] proposed a curve (Fig. 2.2) to determine the value of the turbulence intensity at a reference height 30 m from the ground level for different roughness length. The reference height of 30 m is chosen on the basis that measurements made at this height should free from very local influences but still be representative of the local terrain. The height of 10 m, commonly adopted for meteorological reference measurements, is thought to be very low for many sites. For very rough condition the reference height of 30 m is also very low, but is to be regarded as a reasonable compromise. The estimated variation of turbulence intensity as a function of the roughness length is also shown in the Fig. 2.2. This was derived from

$$\sqrt{\overline{u^2}}/U = \frac{1}{ln\left(\frac{z}{z_0}\right)} \tag{2.5}$$

It can be seen that this expression over-estimates the turbulence intensity for roughness lengths greater than about 0.10 m. It can be seen in the curve that turbulence intensity increases with increase in roughness length. Although more data is needed for terrain types 3 and 4, the proposed variation of the turbulence intensity as a function of roughness length is suggested to be the most representative available.

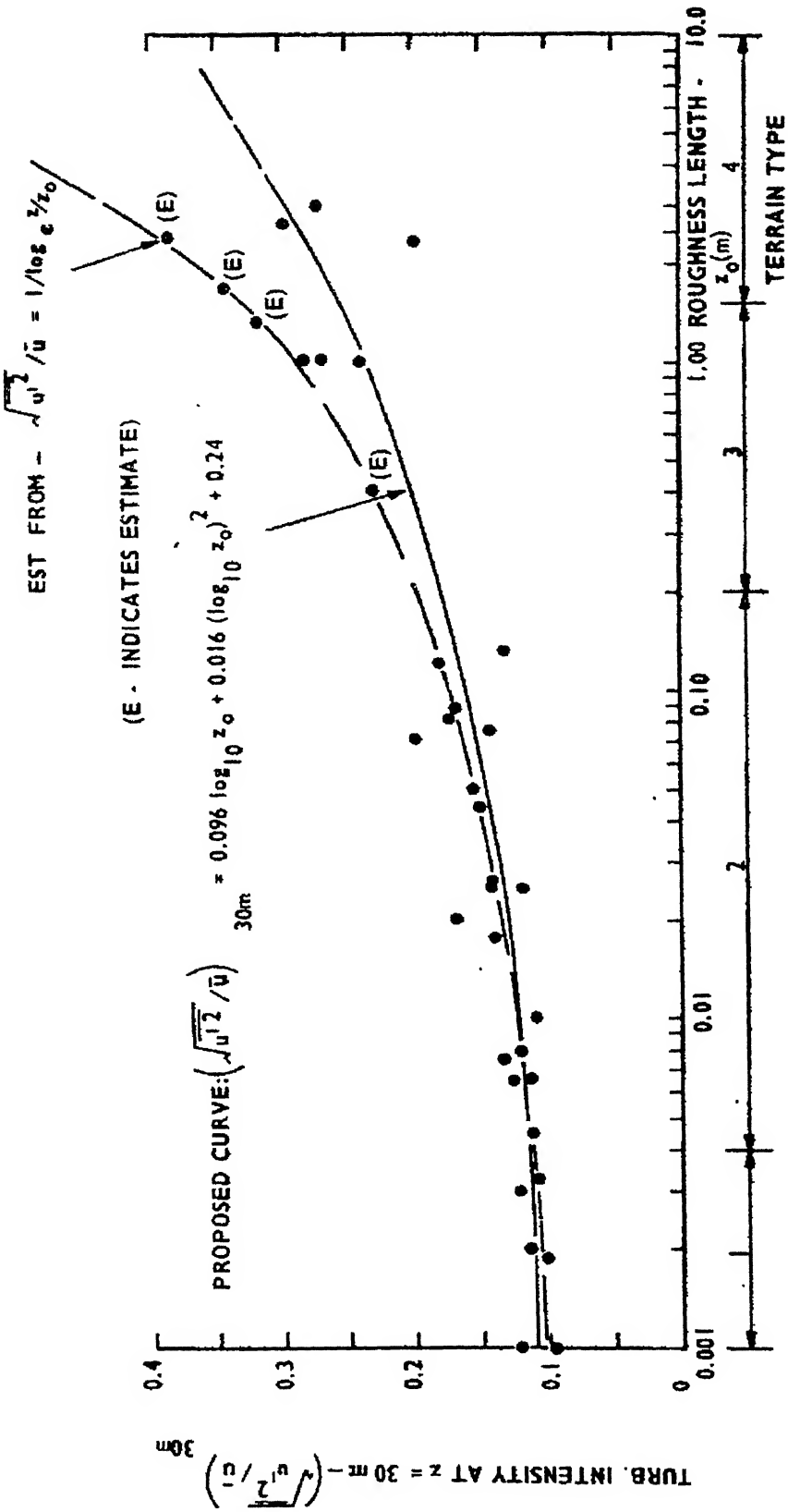

Fig. 2.2 Turbulence intensity at 30 m height for different roghness length

(From Counihan [5])

$Lu_x(m)$	z(m)
11.5	2.0
12-18	2.5
30.0	10.0
70.0	35.0

Table 2.3: Variation of Lu_x with height

2.7 Integral Length Scale

When wind flows over rough terrain, eddies are formed and mean size of these eddies determine what is term as the integral length scale. It is defined by

$$Lu_x = \overline{U} \int_0^T R(\tau) d(\tau) \tag{2.6}$$

The mean eddy size in the longitudinal direction, Lu_x, was first deduced by Taylor (as quoted by Counihan [5]). Taylor found the size of eddies as 70 m at a height of 10 m in his investigation. Recent data suggests a value of the order of 100 m at this height. The mean eddy size increases with increase of height above the ground because it gets more space to expand.

Since integral length scale is a function of height, many authors suggested empirical formulae to estimate its value. All found almost one same range of longitudinal integral length scale for a given height. Some typical results are given in Table 2.3

It was assumed that these length scales are functions only of height and thermal stratification. It was also deduced that it increases with height up to 240 m height and depends upon roughness length. But above this height, the length scales are independent of surface roughness.

Lw_x also increases with height up to about 120 m and then remain constant up to about 370 m height from the ground level. Lw_x is insensitive to changes in terrain roughness, and its variation with the height in the constant shear stress layer can be taken as

$$Lw_x \propto z$$

Counihan [5] proposed a graph (Fig 2.3) to determine the value of integral length scale with height (>10 m) for different roughness lengths, corresponding to four different terrains. It can be seen in this graph that the value of integral length scale increases with height up to 240 m in the atmospheric boundary layer, but above this height it decreases and is independent of roughness length. Below 10 m, height it can be assumed that Lu_x decreases rapidly with decrease of height. He also proposed a graph to determine the value of integral length scale at a reference height 30 m for different values of roughness length.

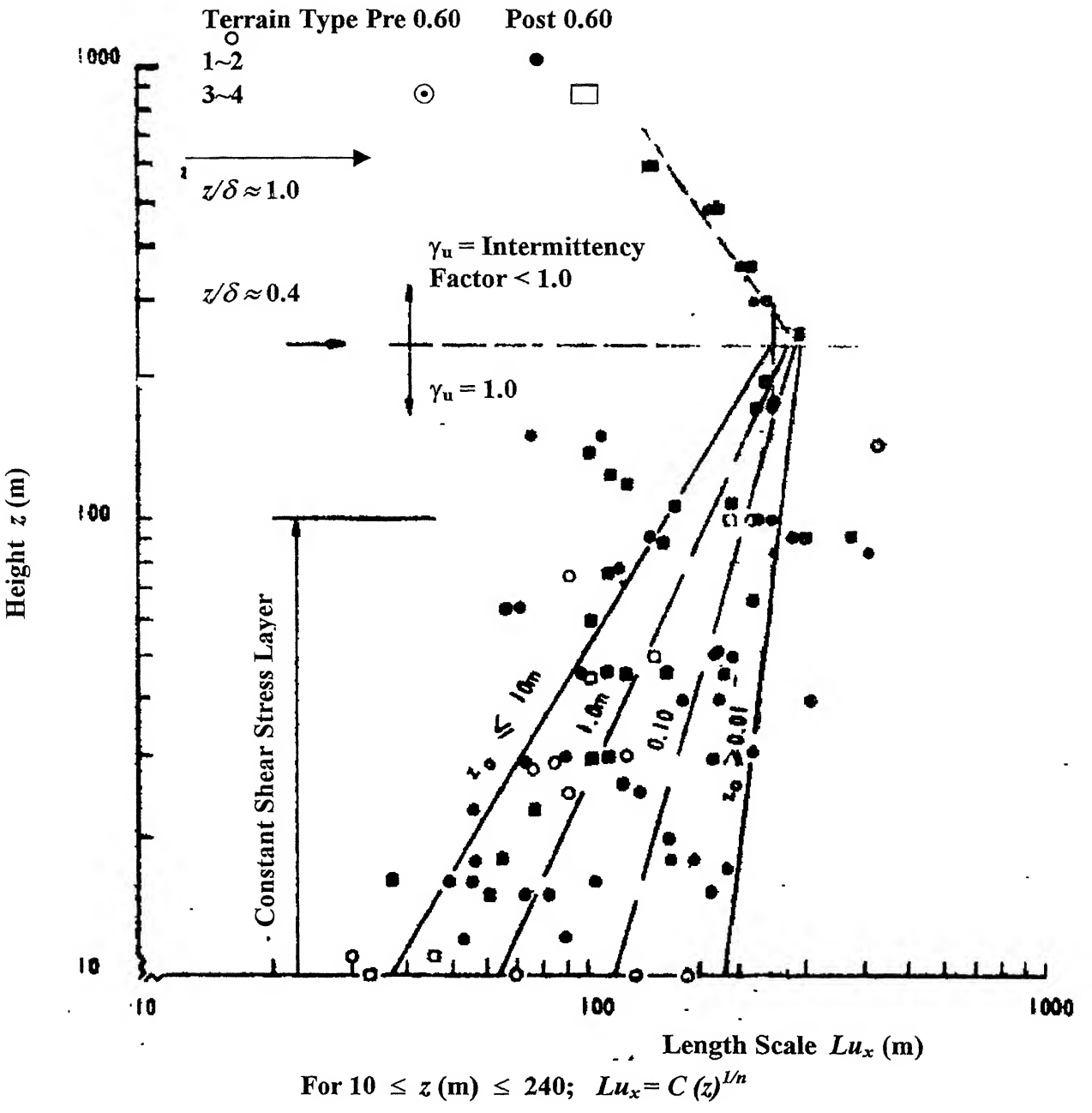

Fig. 2.3 Variation of length scale with height and roughness length (From Counihan [5])

He also suggested a formula to measure the value of Lu_x at 30 m height.

$$Lu_x = 108\left(\frac{1}{z_0}\right)^{1/6} \tag{2.7}$$

In Fig 2.3, the positions of the lines for various values of the roughness length were again based on the data that were considered to be the most accurate and reliable. It was assumed that these lines should tend to converge at some height, and that above this height integral length scale would be independent of terrain roughness. This height was assumed to be in the region where the intermittency factor begins to decrease in value from unity; this is of the order of 240 m. The few measurements above 240 m agree with flat-plate data, which indicate that the turbulence length scale should then decrease with further increase of height.

Counihan [5] proposed another graph (Fig. 2.4) with varying roughness length for a height Variation of integral length scale with roughness length. upto 240 m height range of 10 m-240 m. Integral length scale in this height range for any roughness length can be derived from

$$Lu_x = C(z)^1/n \tag{2.8}$$

The values of C and $1/n$ can be obtained by the Fig. 2.4. It was concluded that the variations of integral length scale with roughness length and height deduced here are the most consistent and reliable based on the available data, despite the lack of agreement with previous predictions.

LENGTH SCALE $Lu_x = C(z)^{1/n}$

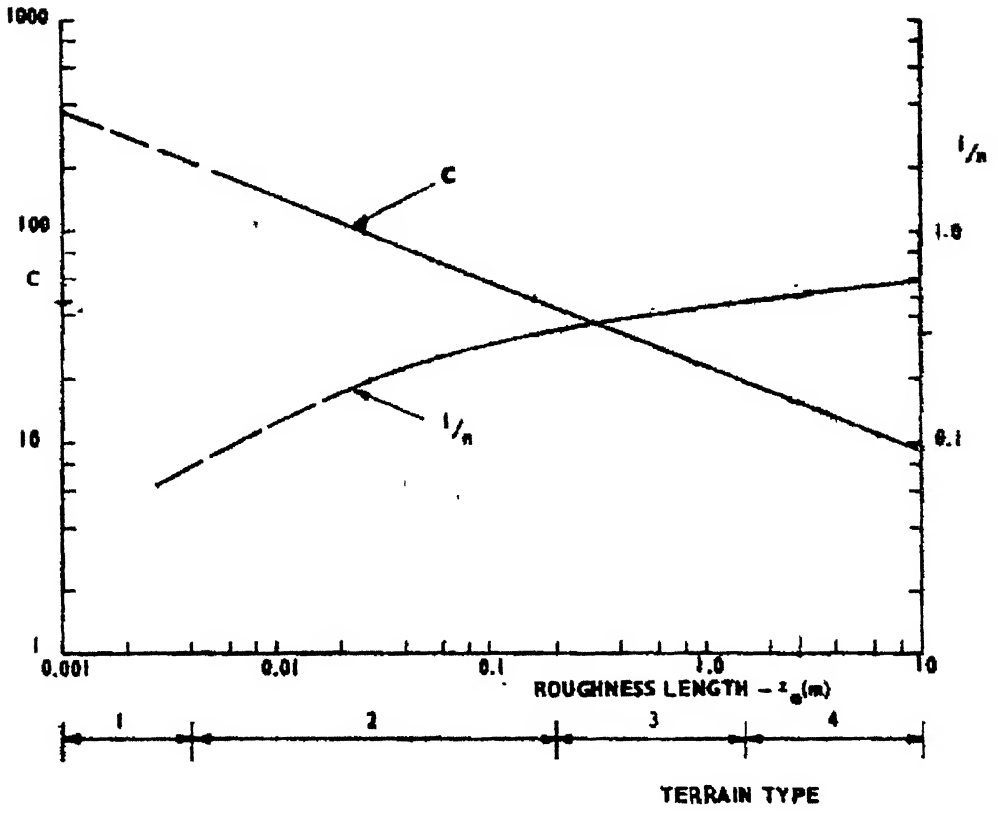

Fig. 2.4 Variation of C and $1/n$ with Roughness Length

(From Counihan [5])

Chapter 3

Experimental Set-up

This chapter gives an overview of the test facility, describes the experimental arrangement, the measurements carried out in the present investigation and various techniques developed for the purpose.

3.1 Test Facility

The return circuit closed test-section subsonic wind-tunnel, which is located in National Wind Tunnel Facility (N.W.T.F.) of the Aerospace Engineering Department, Indian Institute of Technology, Kanpur, is used for the present experimental investigation. Its current maximum speed is 80 m/s and Reynolds number is 6×10^6/m. Some characteristic features of this tunnel are as follows:

1.	Interchangeable test section	
	Cross section	3 m×2.25 m
	Length	5.75 m (upstream part) + 3 m (downstream part)
2.	Contraction ratio	9:1
3.	Max. wind speed	80 m/s
4.	Reynolds No.	6×10^6 / m
5.	Guide vanes	Simple circular type
6.	Honeycomb	Hexagonal
7.	Anti-turbulence screens	4
8.	Turbulence level	< 0.1 %
9.	Flow angularity	< 0.20

It can be seen that this is a very high quality wind tunnel specially designed for transport aircraft work. The length of the test section is not sufficient for any meaningful boundary-layer depth to occur over the test location.

We, therefore, have to use artifices to make the boundary layer grow. Various techniques have been suggested to obtain the required velocity profile in the short test-sections of aerodynamic wind tunnels. One of the method recommended by Gupta and Yadav [8] is to extend the test-section floor into the contraction cone and to provide a slot into this

extended floor. The air blowing through the slots injects excess momentum towards the top of the test-section. The other standard methods of producing momentum deficit at the lower end include properly placed barriers in the early part of the test-section.

3.2 Simulation Hardware

Several devices were used to simulate the atmospheric boundary layer. The extension of the test-section floor into the contraction cone, barriers and spires were all used. Specifications of the devices are described here step by step.

3.2.1 Slots

Three $\frac{3}{4}$ inches thick and 3.4 m long boards were used in the contraction zone to extent the test-section floor. Two slots of 10.0 cm wide were provided in the boards in the inner region of the contraction zone. Due to these slots, air blowing through the slots in the tunnel floor injected momentum directly towards the top of the boundary layer. A slight variation in the velocity was found in the upper velocity profile.

3.2.2 Barriers

The main purpose of barriers is to produce initial momentum deficit near the ground level in order to account for the smaller roughness length down-stream. Three flow features, namely, (1) a separation bubble downstream. (2) a shear flow along the bubble boundary. (3) a pressure gradient down-stream are produced by barriers in the wind tunnels. These flow features are usually not consistent with the naturally-grown boundary layer. First two effects are detrimental but unavoidable; the separation bubble effectively nullifies the effect of surface friction in the bubble region between the barrier and down wind of the bubble, the shear layer contains the Reynolds stresses concentrated at the barrier height and requires mixing into the boundary to give correct distribution. Both these effects can be reduced by the modification of the barrier, which consists of perforating or castellating the edge. On the other hand, the adverse pressure gradient is advantageous, since it prompts the growth of the boundary layer. As already mentioned, none of these three characteristics is consistent with the naturally grown boundary layers. To reduce the negative effects to the minimum possible, a stretch of the roughness element is used so as to decay these characteristics and allow the boundary layer to recover before it is used. Three barriers of size 10 cm. each, were used in this investigation. All three barriers were mounted on the spires, with a spacing of 10.0 cm. between two at the beginning of the upstream as shown in Fig. 3.1.

3.2.3 Spires

Five tapered wooden spires of identical geometry were mounted at the beginning of the test-section as shown in Fig. 3.1. The principle purpose of the spires is as vorticity generators. But the tapered shape is also responsible for creating a momentum deficit near the bottom of the tunnel-section. The main purpose of spires is, of course, to generate turbulence by acting as a vorticity generator. An inner turbulent shear layer was then developed over an array of roughness elements of appropriate size and density to produce a flow having the desired mean velocity profile and turbulence structure. Barriers in conjunction with the spires were also used to develop a boundary layer of adequate depth and desired characteristics.

All dimensions of the spires were obtained by keeping the total blockage and rate of decrease of area with height same as in Ref. [2]. The height of the spires was chosen to maximize the boundary layer thickness.

3.2.4 Roughness elements

Roughness elements were used to rougher the ground and model the natural boundary layer. As has been mentioned before, the matching of the prototype and the model factor in the atmospheric boundary layer experiments depends to a very large extent on proper scaling of the turbulence characteristics. For example, the length scale of turbulence must be as close to the physical length scale as possible. In fact, satisfactory modeling requires that the model physical length scale factor should be close to match the scale factor of the turbulence related lengths.

In this work we determine the scale factor for turbulence related lengths and then prescribe them as model scale factor.

It is the endeavor of most of the experimental work to reduce the scale factor of the turbulence related lengths so that larger models could be used in wind tunnel.

Seventy-two roughness elements having a cross-section of 17 cm x 17 cm., were mounted perpendicular on five half-inch thick, 8 x 4 feet wooden boards in twelve staggered rows, at a spacing of 41.0 cm. Boards were also screwed on the test-section of the wind tunnel. Spacing between two plates in a row was kept 32.6 cm and two rows were 41 cm apart. All roughness elements were mounted on the entire test-section of the wind tunnel, which was 5.75 m long and 3.0 m wide. Only one-meter space was left at the start of the test-section for the installation of the spires and the barriers. All readings had been taken after 1.5 m. distance from the last row which was almost nine times height of the their size so that wakes generated by roughness elements would not produce much effect at the test-section. Staggered rows were preferred from the other arrangements because it could produce more turbulence.

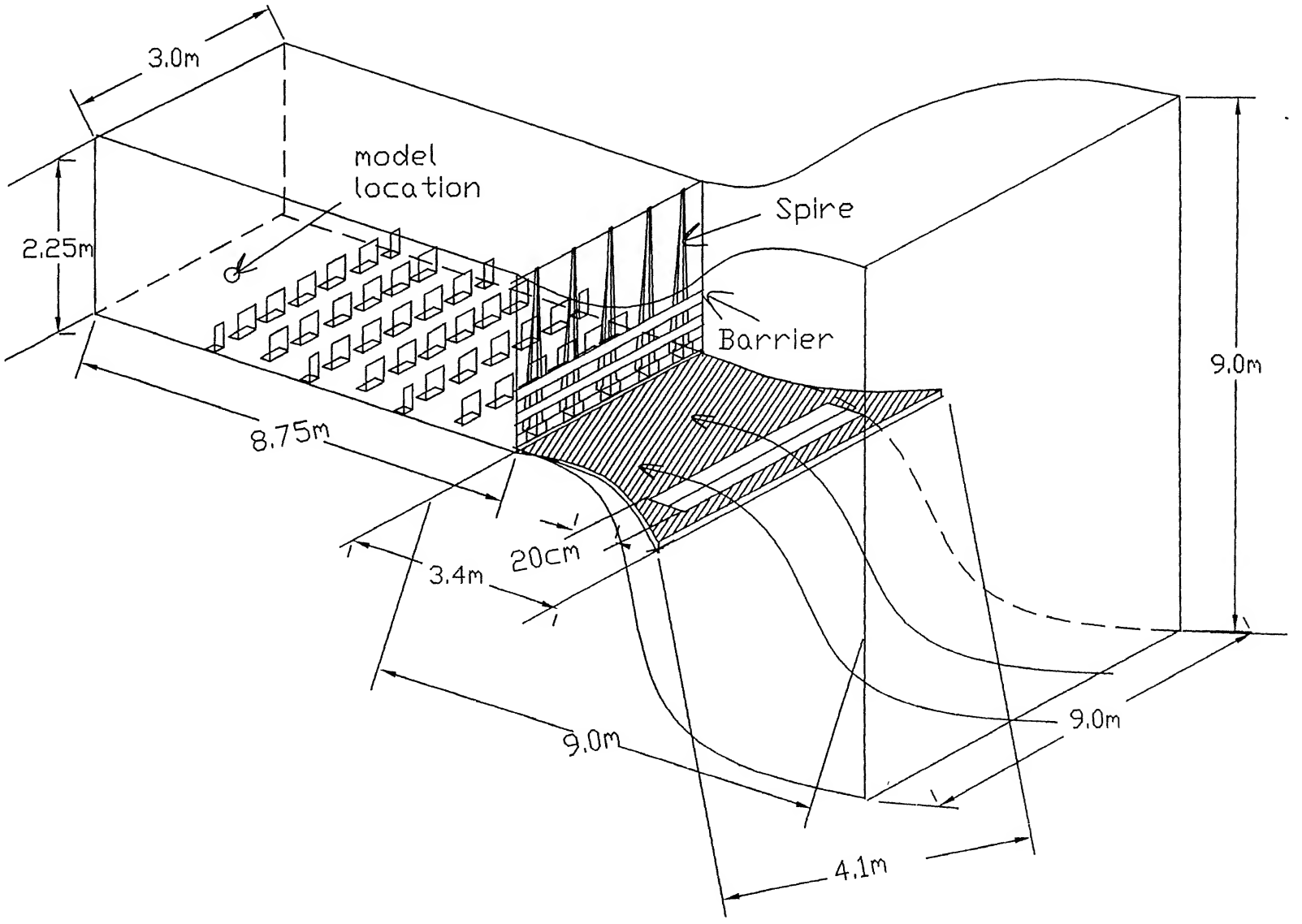

Fig. 3.1 Typical experimental set-up of simulation hardware

Sensor resistance, R_{20}	9.30 Ω
Sensor lead resist.,R_L	0.70 Ω
Support resistance, R_s	0.05 Ω
Desired wire temp., T_W	250 C
Temperature of flow, T_0	25 C
Operating resist., R_W	10.08 Ω
Total resistance,R_T	10.05 Ω
Overheat ratio, a	0.80
Probe body diameter	2.0 mm
Support needle length	30.0 mm
Needle base diameter	2.5 mm
Needle tip diameter	0.2 mm
Spacing between needles	3.0 mm
Sensor length	3.0 mm

3.3 Hot-Wire Probe

A conventional single wire hot-wire probe with following wire properties is used for acquiring the velocity data. The sensor for the hot wire used in the present investigation is made of wollaston platinum rhodium (90/10) wire joined to the prongs by etching and soft soldering. Characteristics of hot-wire probe is described above.

3.4 Data Aquisition

In the present study DANTEC streamline DT-11, code-9090N0101, Serial No. 239, CTA (Constant Temperature Anemometer) was used to acquire the velocity signals at a desired sampling rate of 60000 samples per second and store the samples in the hard disk in binary format.

The basic analog input considerations are

- Sampling rate
- Resolution
- Input range

Sampling Rate - This parameter determines how often analog to digital conversions can take place. A faster sampling rate acquires more points in a given time and can therefore often form a better representation of the original signal. To properly digitize this signal for analysis, the Nyquist sampling theorem stipulates that the sampling rate must be more

than twice the rate of maximum frequency component to be detected. In the present investigation a sampling rate of 60000 sample per second was taken.

Resolution - The number of bits that the ADC uses to represent the analog signal is the resolution. The higher the resolution, the higher the number of divisions the range is broken into, and therefore, the smaller the detectable voltage changes. A 12-bit converter divides the analog range into 4096 divisions. By increasing the resolution to 16 bits, however, the number of codes from the ADC increases from 4096 to 65,536, and one can therefore obtain an extremely accurate digital representation of the analog signal, if the rest of the analog input circuitry is designed properly. But in the present study the resolution of the DAC is 12 bit and therefore 4096 divisions.

Range - Range refer to the minimum and maximum voltage levels that the ADC can quantize. The multifunction DAQ boards offer selectable ranges so that the board is configurable to handle a variety of different voltage of different voltage levels. With this flexibility, one can match the signal range to that of the ADC to take best advantage of the resolution available to accurately measure the signal.

The range, resolution, and gain available on a DAQ board determine the smallest detectable change in voltage. This change in voltage represents 1 LSB of the digital value, and is often called the code width. The ideal code width is found by dividing the voltage range by gain *times* two raised to the order of bits in the resolution. In the present case the resolution of the DAQ board is 12 bit, has a voltage range of 0 to 5 V and gain of 5. Ideal code width, therefore, is given by

$$\frac{5}{12} \times 2^{12} = 0.61\mu V$$

Therefore, the theoretical resolution of one bit in the digitized value is $0.61\mu V$.

3.4.1 Software

The software required for the sampling was developed using the application tool LabVIEW. In this software we can select the number of channels, sampling rate, buffer size and the minimum number of scans to write at a time on the hard disk. In addition to the above we can supply the use header, which we can use for identification of the sampling parameters during the analysis.

3.5 Velocity Measurement

A hot-wire P-11 probe connected with DANTEC streamline Instrument, calibrated with a LabVIEW program was used to obtain velocity time series, mean velocity and r.m.s. velocity. A thin wire which is made of tungsten having a diameter of 5μ, is used to connect the heads of hot-wire probe. The probe, connected with a probe holder and the

holder was mounted on the automatic traversing system. A pitot-static pressure probe in conjunction with a manometer was also used to measure the free stream velocity. The pitot-static probe was also placed at the same traversing system parallel to the hot-wire probe. A VI program was made to measure the mean velocity and the r.m.s. velocity.

3.6 Traverse Mechanism

An automatic 3-axis traversing mechanism was used for traversing the hot-wire probe. It had three-translation degree of freedom with maximum possible displacement of 8.75 m, 2.8 m, and 1.70 m in the stream-wise, span-wise, and vertical directions respectively. Its positioning accuracy is ± 0.1 mm over entire range. Traversing was done by using a computer program. Computer had two options to traverse the probe, first manually and second automatic. Because computer was unable to take more than 20 points each time, so traversing was done by manual setting of the points in the program.

3.7 Measurement of Turbulence Intensity and Integral Length Scale of Streamwise Turbulence Component

Wind speed varies randomly with time. This variation is due to the turbulence of the wind flow. Velocity fluctuations in a flow passing a point may be considered to be caused by a superposition of eddies transported by the mean wind. The simplest descriptor of atmospheric turbulence is turbulence intensity.

3.7.1 Turbulence intensity

The 'intensity' of turbulence is a measure of amplitude of the velocity fluctuations, which occur in the flow.

$$TurbulenceIntensity = \frac{\sqrt{\overline{u^2}}}{\overline{U}} \times 100 \tag{3.1}$$

The intensity of turbulence is proportional to the angular velocities of the eddies. The eddies of same size may produce different intensities of turbulence, depending upon their rotational speeds. The energy content of a large eddy is much greater than that of a smaller one for a given intensity, and energy is transferred from larger eddies to smaller ones.

3.7.2 Integral Length Scale

Each eddy is viewed as causing at that point a periodic fluctuation with circular frequency $\omega = 2\pi n$. By analogy with the case of the traveling wave, the eddy length is $\lambda = \frac{U}{n}$. Eddy wave number is $k = \frac{2\pi}{\lambda}$, Wavelength is a measure of eddy size. To obtain the integral length

scale, the random behavior of a fluctuating velocity at a particular point in space has been a point of discussion. For small objects near that point, it would be reasonable to assume that the values obtained for wind force, say, due to the gustiness were fairly representative of those experienced over the whole object.

But for large constructions such as low-rise buildings, bridges or towers, there is no longer the cause and there can be no direct relationship between the random behaviors of the wind from place to place along the structure. It is nonetheless necessary to obtain a measure of the distribution of the gusts, say, along a building and statistical method must be employed. Integral length scales of turbulence are measures of the average size of the turbulent eddies of the flow. There are altogether nine integral scales of turbulence, corresponding to the three dimensions of eddy associated with the longitudinal, traverse and vertical components of the fluctuating velocity. But in the present investigation single hot-wire probe was used which was able to measure longitudinal component of the turbulence.

Lu_x is the measure of the average longitudinal size of eddies associated with the longitudinal velocity fluctuations.

To get integral length scale, auto-correlation coefficient is used in this investigation.

To get the idea of the length scales of the fluctuating motion, the correlation between the same fluctuating quantities measured at two different points in space. Suppose two points have co-ordinates x and $x+r$, then the covariance of the u-component in defined as $\overline{u(x)u(x+r)}$, a function of x and r in general.

Then auto-correlation coefficient is

$$R_{uu}(x) = \frac{\overline{\left[U_{(x)} - \overline{U}_{(x)}\right]\left[U_{(x+r)} - \overline{U}_{(x+r)}\right]}}{\sqrt{\overline{u_x^2}\,\overline{u^2}_{x+r}}} \tag{3.2}$$

The correlation with separation is a measure of the strength of eddies whose length in the direction of r is greater than the magnitude of r. Taylor's formula for integral length scale is adopted in this work. According to him Integral length scale is

$$Lu_x = \overline{U}\int_0^T R(\tau)d(\tau) \tag{3.3}$$

Area under the curve of R(τ) gave time scale which on further multiplication with mean velocity produced integral length scale. Estimates of turbulence scales depend significantly upon the length and the degree of stationary of the record being analyzed and usually vary widely from experiment to experiment.

But this requires velocity measurements at two locations simultaneously. Using ergodic theorem, it is possible to convert this into auto-correlation with time delay. Thus, we define auto-correlation coefficient as

$$R_{uu}(\tau) = \frac{\overline{\left[U(t) - \overline{U}(t)\right]\left[U(t+\tau) - \overline{U}(t+\tau)\right]}}{\overline{u^2}} \tag{3.4}$$

Chapter 4

Result and Discussion

Eighteen configurations of three artificial devices i.e., spires, barriers, and slots and two type of surface roughness were used for the present investigation as presented in Table 4.1. With each configuration, variations of mean velocity, streamwise turbulence intensity and longitudinal length scales of streamwise turbulence with increasing height were measured. Computer-operated traverse system was used to traverse the hot-wire probe along z-direction. Readings were taken at thirty vertical locations. The Reynolds number corresponding to the longitudinal length scales and free stream velocity used throughout the investigation is of the order of 10^6.

4.1 Data Analysis

4.1.1 Mean-Velocity Profiles

The raw mean velocity profiles of some of the configurations are shown in Figures 4.1-4.4. The mean velocity at any location z_0 is the arithmetic average of 32,000 data points (0.533 sec). To present the data in standard non-dimensional forms we need the value of shear velocity u^*. This was not measured directly. However, A.E. Perry and P.N. Joubert [9] have suggested the following method of determining the value of shear velocity and average roughness length. He assumes the log-law for the velocity profile in the form

$$\frac{U}{u^*} = \frac{1}{k} ln \left(\frac{z}{z_0} \right) \tag{4.1}$$

where z_0 is reference roughness length. This can be written as

$$\frac{U}{U_R} = 5.6 \frac{u^*}{U_R} log \left(\frac{z U_R}{v} \right) - 5.6 \frac{u^*}{U_R} log \left(\frac{z_0 U_R}{v} \right) \tag{4.2}$$

where U_R is the reference velocity taken at any convenient height. We take here U_R as the value of the mean velocity at a height of 1 m. in the wind-tunnel. With this as a reference height, we calculate U/U_R and plot against $log(zU_R/n)$.

Configur-ation No.	Surface Roughness (*)	Barrier Height(**) mm	Spires 5	Slot mm.
1.	F.R	300	YES	0
2.	F.R	200	YES	0
3.	F.R	100	YES	0
4.	F.R	300	YES	100
5.	F.R	200	YES	100
6.	F.R	100	YES	100
7.	F.R	300	YES	200
8.	F.R	200	YES	200
9.	F.R	100	YES	200
10.	H.R	300	YES	0
11.	H.R	200	YES	0
12.	H.R	100	YES	0
13.	H.R	300	YES	100
14.	H.R	200	YES	100
15.	H.R	100	YES	100
16.	H.R	300	YES	200
17.	H.R	200	YES	200
18.	H.R	100	YES	200

(*) F.R. = Full Roughness elements (72 elements)
H.R. = Half Roughness elements (36 elements)

(**) Barrier height of 200 mm. represents two planks of 100 mm. each with a gap of 100. mm. between the two.
Barrier height of 300 mm. represents three planks of 100 mm. each with a gap of 100. mm. between the two adjacent ones.

Table 4.1: Various configurations of passive devices

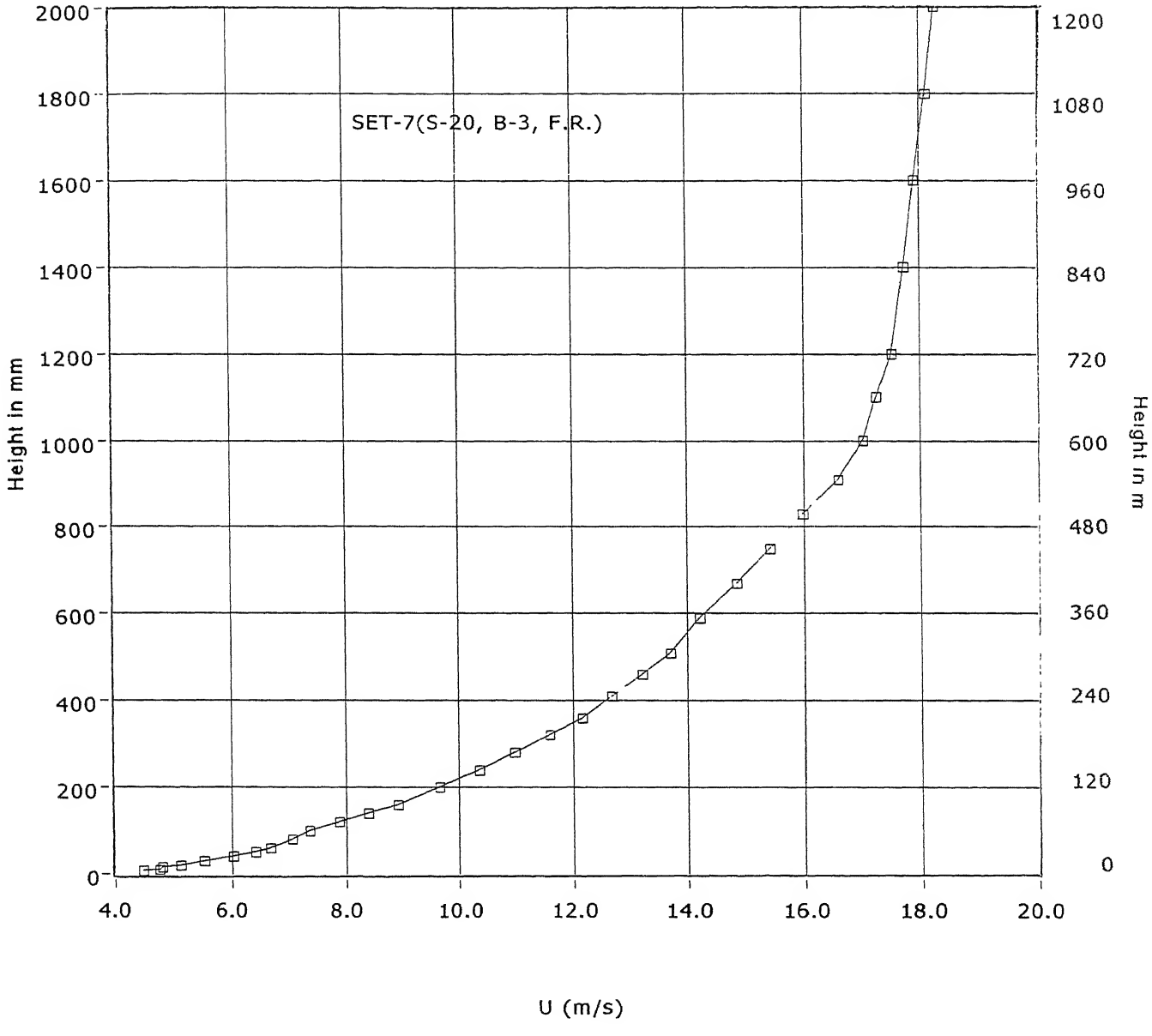
SET-7(S-20, B-3, F.R.)
Height in mm
Height in m
U (m/s)
2000
1800
1600
1400
1200
1000
800
600
400
200
0
1200
1080
960
840
720
600
480
360
240
120
0
4.0
6.0
8.0
10.0
12.0
14.0
16.0
18.0
20.0

Fig. 4.1

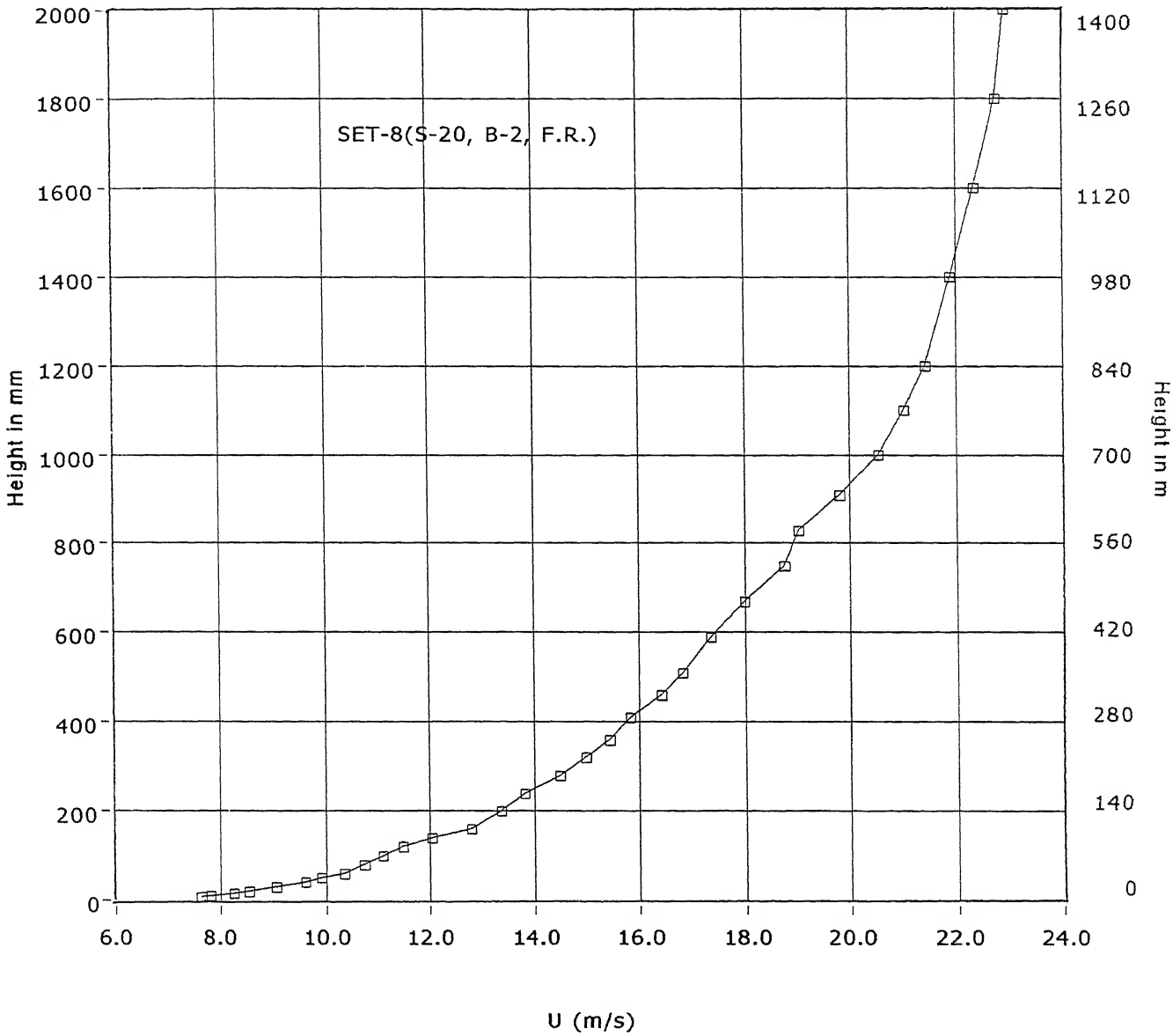
SET-8(S-20, B-2, F.R.)
Height in mm
Height in m
U (m/s)
2000
1800
1600
1400
1200
1000
800
600
400
200
0
1400
1260
1120
980
840
700
560
420
280
140
0
6.0
8.0
10.0
12.0
14.0
16.0
18.0
20.0
22.0
24.0

Fig. 4.2

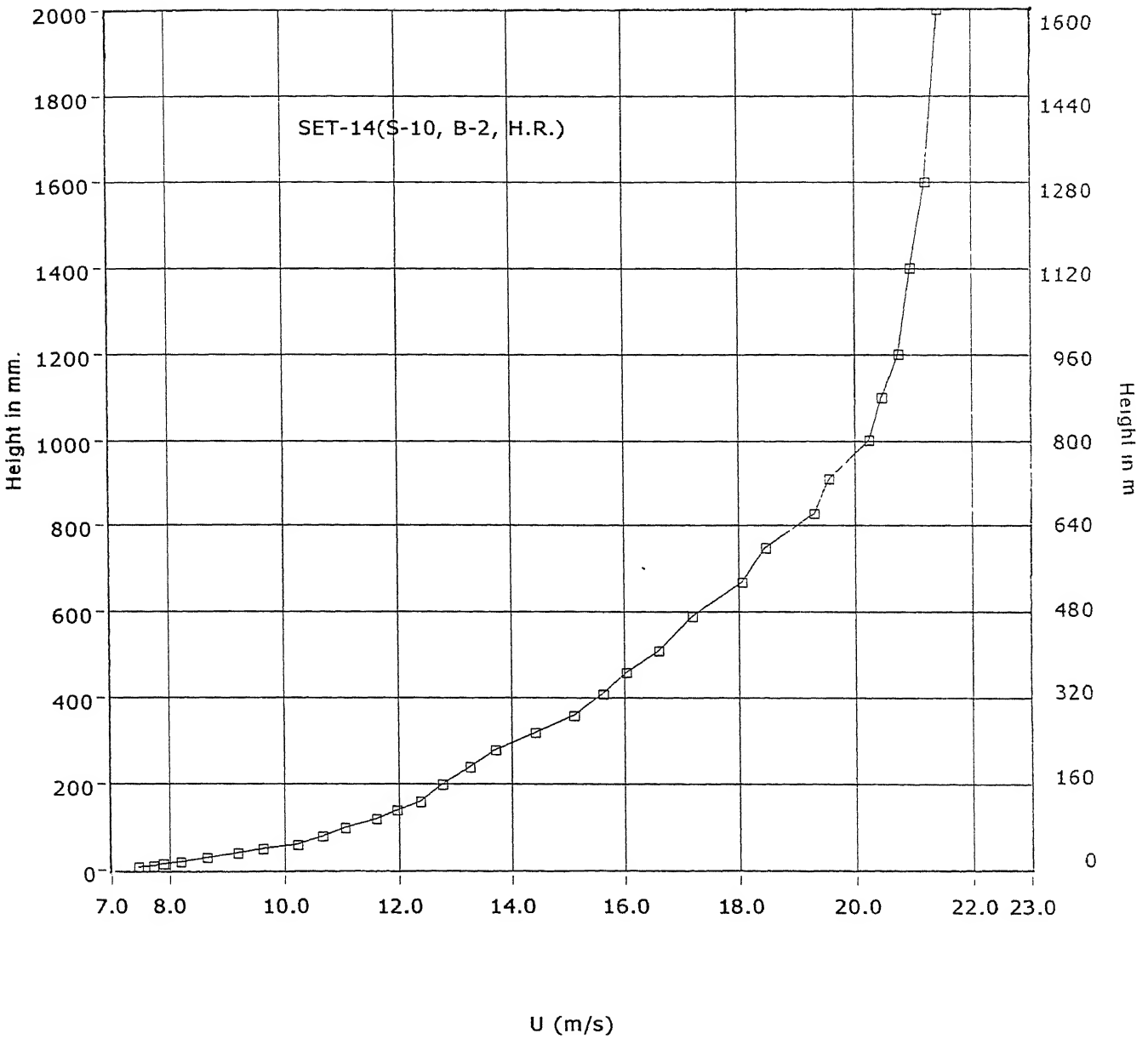
SET-14(S-10, B-2, H.R.)
Height in mm.
Height in m
U (m/s)
2000
1800
1600
1400
1200
1000
800
600
400
200
0
1600
1440
1280
1120
960
800
640
480
320
160
0
7.0
8.0
10.0
12.0
14.0
16.0
18.0
20.0
22.0
23.0

Fig. 4.3

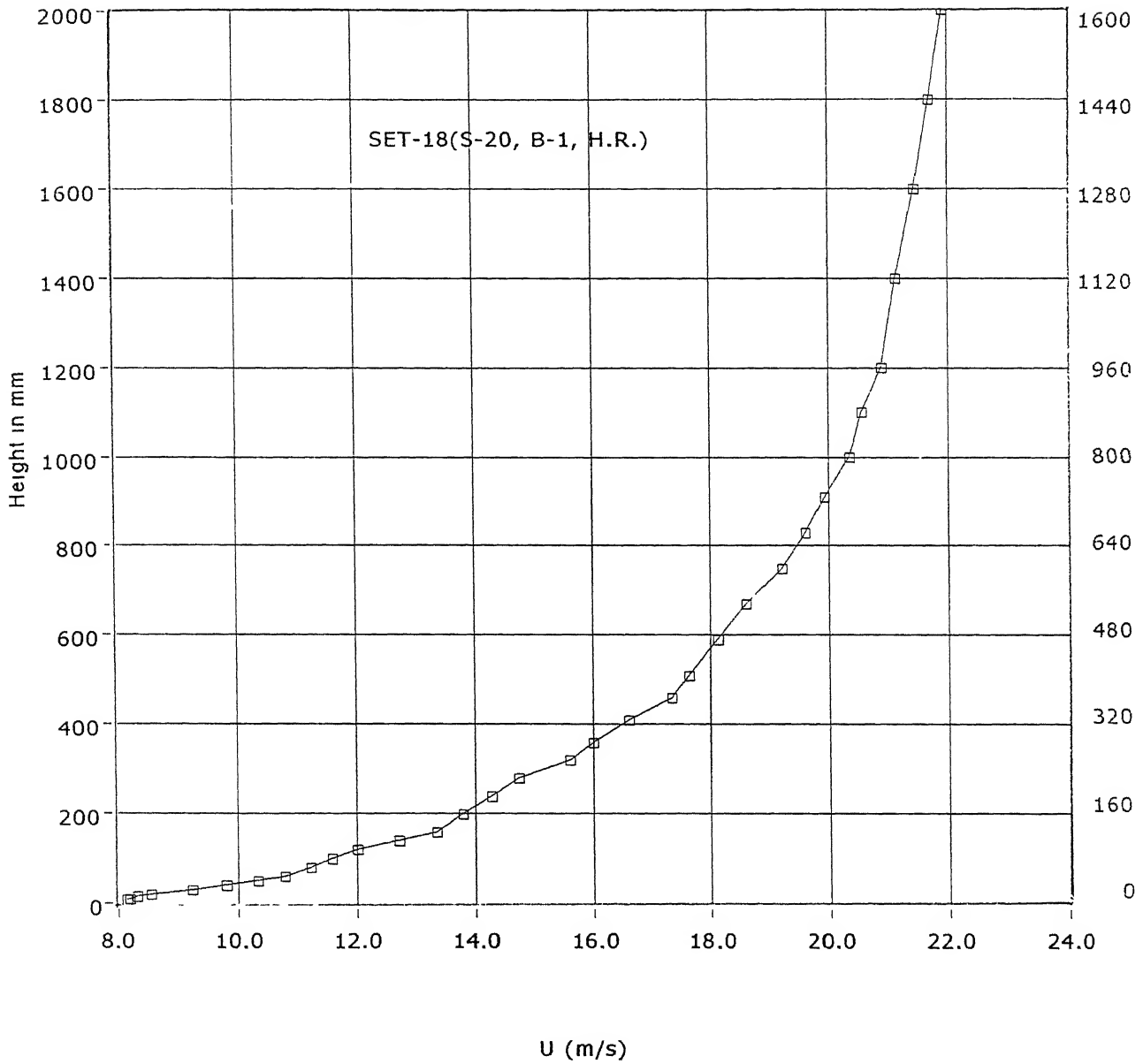
SET-18(S-20, B-1, H.R.)
Height in mm
Height in m
U (m/s)
2000
1800
1600
1400
1200
1000
800
600
400
200
0
1600
1440
1280
1120
960
800
640
480
320
160
0
8.0
10.0
12.0
14.0
16.0
18.0
20.0
22.0
24.0

Fig. 4.4

The value of u^* is then obtain by equating the slope of the best fit line for the upper data with $5.6u^*/U_R$. The value of z_0 is obtain from the intercept with the Y-axis by equating it to $(5.6\frac{u^*}{U_R})log(\frac{z_0 U_R}{n})$ as is clear from Eq. 4.2.

Table 4.2 gives the value of u^* and z_0 obtain for all the configuration tested.

Figures 4.5-4.22 show the log-law representation of the mean velocity profiles for various configurations in terms of U/u^* and $log(z/z_0)$. For all configurations, the values of aerodynamic roughness parameter, z_0 are found of the order of 10^{-3} m order. Surface roughness is an important parameter in the wind tunnel to simulate z_0.

All log-law representations of the mean velocity profile with full surface roughness show a logarithmic law of the wall region with a distinct 'velocity-defect' or 'wake' region above. With increase in barrier height the wake region becomes less distinct and log law extends over a larger height near the wall. The variation of z_0 with the barrier height can be seen in the Figures 4.5-4.22. z_0 increases with increase in barrier height.

The increase of surface roughness makes the 'defect region' of 'wake' more distinct, which is consistent with the naturally grown boundary layers.

We also calculated the power-law indices for the velocity profile based on the form

$$\frac{U}{U_R} = \left(\frac{z}{z_R}\right)^{1/\alpha} \tag{4.3}$$

was used to fit the data. Taking log on both the sides, we get

$$\log\left(\frac{U}{U_R}\right) = \frac{1}{\alpha} log\left(\frac{z}{z_R}\right) \tag{4.4}$$

slope of $log(\frac{U}{U_R})$ vs $log(\frac{z}{z_R})$ will give the value of $1/\alpha$. Tieleman et.al. [2] have proposed a two-layered model for the wind-tunnel boundary layer simulated artificially by barriers, spires and roughness elements. Taking after them we use a two-layered model, the lower layer extending to about 10 cm. in the wind tunnel. The power indices $1/\alpha$ calculated for the two layers are given in the Table 4.3. Note that the $1/\alpha$ value for the lower velocity profile compares very well with the Tilemen's value of 0.12. The value for the upper layer, which Tielemen reported as between 0.27 to 0.29 also compares well. This also compares favourable with the values reported by Counihan [5] for the natural boundary layer on many of the world cities. The range represented there varies from 0.26 for London, U.K. to 0.31 for Minneapolis, USA, which is rather a flat city.

Figures 4.23-4.40 show the power-law representation of the mean velocity profiles for various configurations. For all configurations it was observed that the boundary layer had different exponents for upper and lower regions. Upper regions show poor power-law representations. The representations improve with the increase in the barrier height and with the shift in the axial location of measurement station from bottom to roof to the tunnel.

S.No.	u*(U.P) m/sec	z_0(U.P) mm
1.	1.451	6.38
2.	1.553	4.68
3.	1.548	3.84
4.	1.462	6.51
5.	1.563	4.91
6.	1.568	4.12
7.	1.474	6.91
8.	1.601	5.18
9.	1.611	4.72
10.	1.406	4.116
11.	1.421	2.37
12.	1.431	2.08
13.	1.461	4.28
14.	1.428	2.46
15.	1.44	2.44
16.	1.400	4.41
17.	1.431	2.95
18.	1.429	2.56

Table 4.2: Calculation for Model Scale Factor

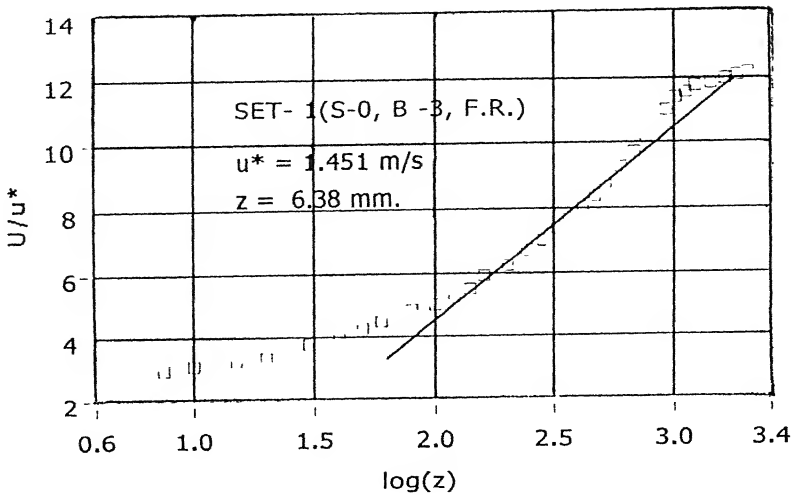

Fig. 4.5

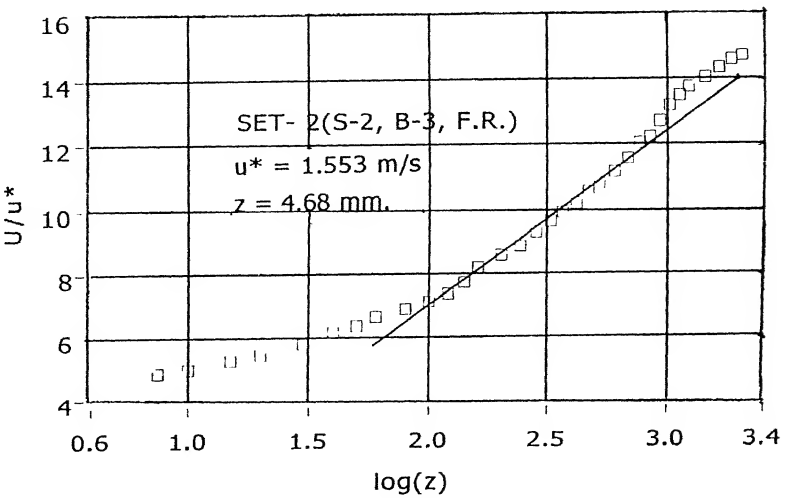

Fig. 4.6

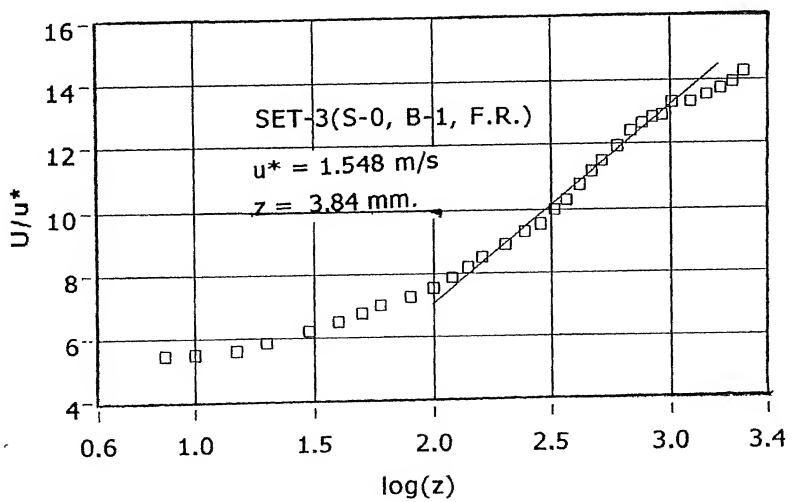

Fig. 4.7

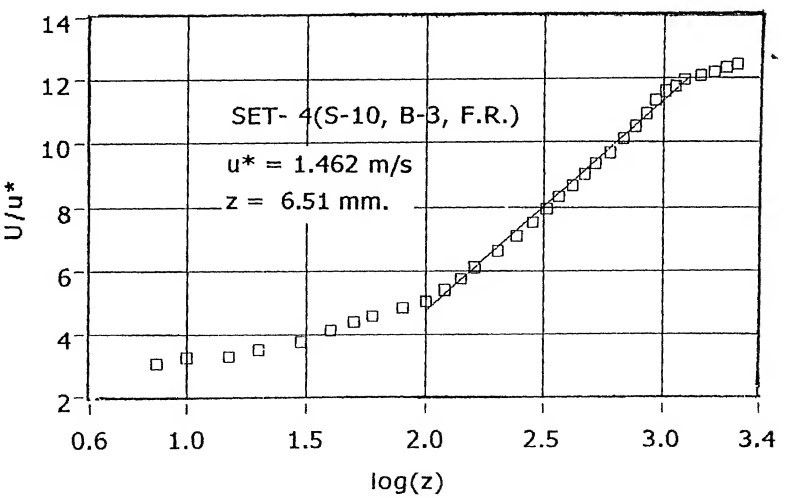

Fig. 4.8

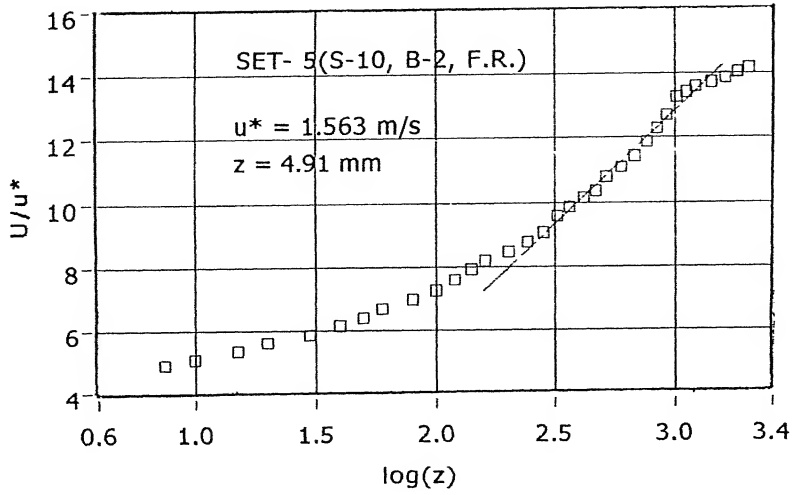

Fig. 4.9

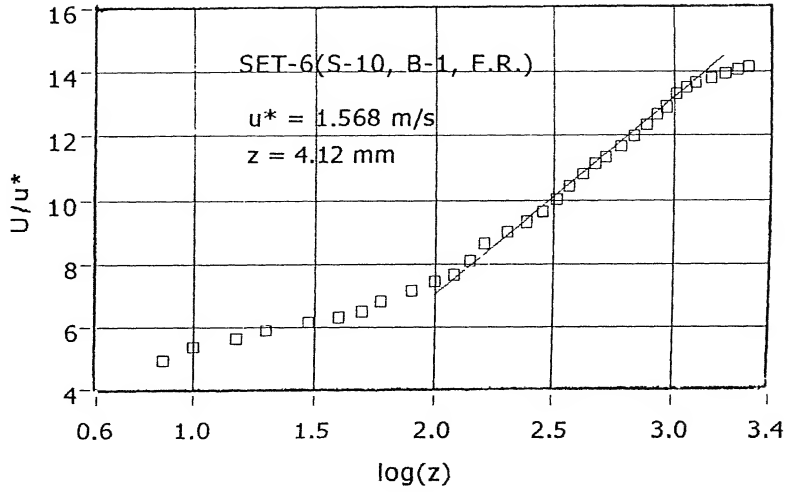

Fig. 4.10

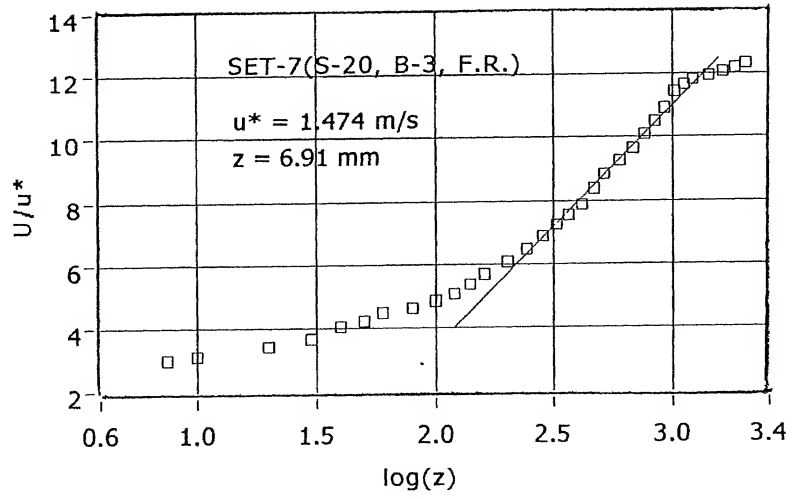

Fig. 4.11

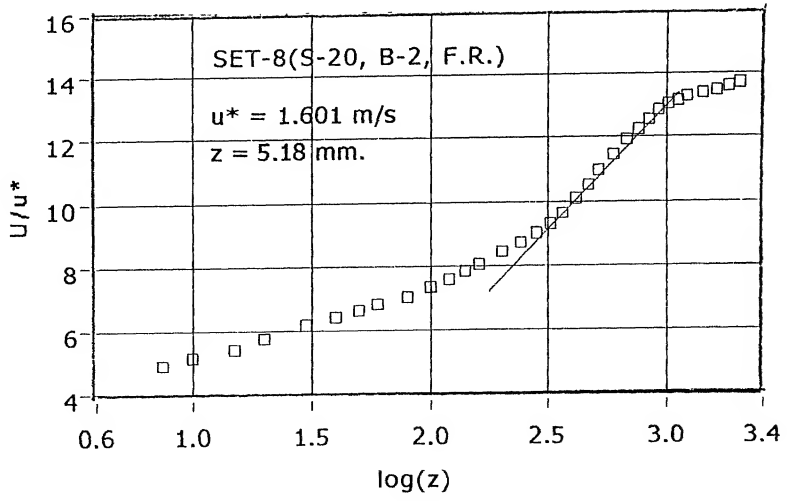

Fig. 4.12

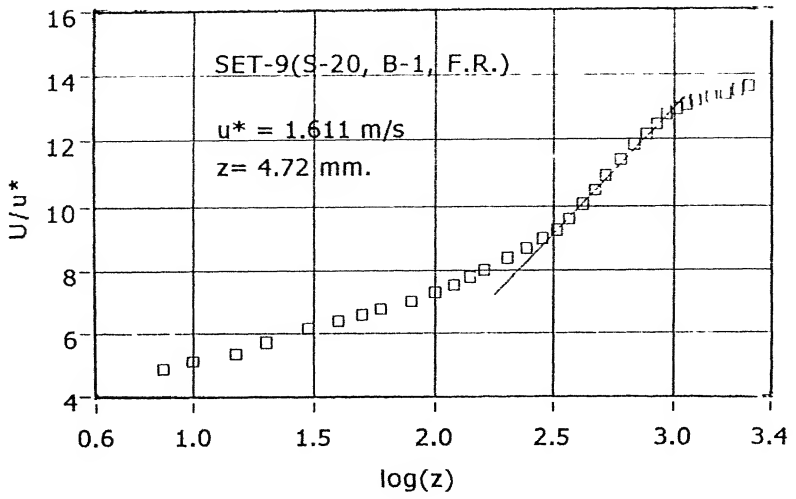

Fig. 4.13

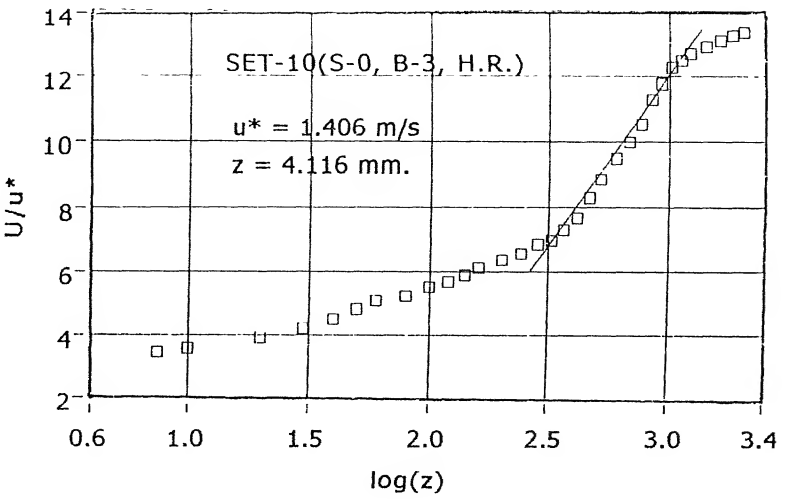

Fig. 4.14

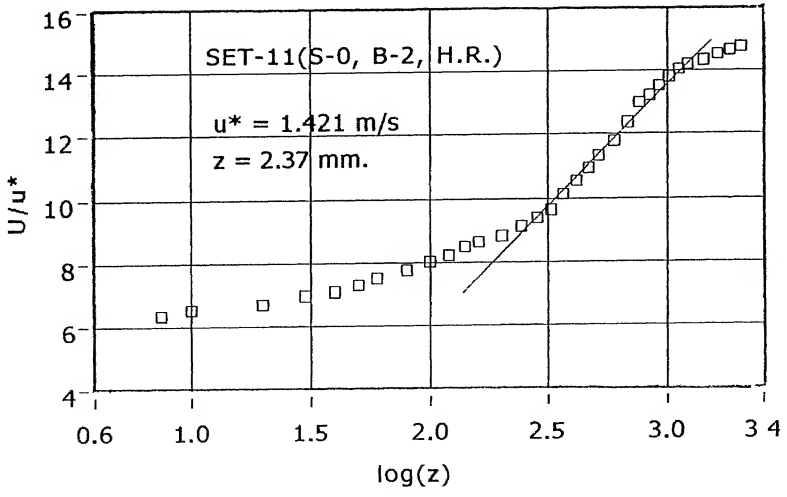

Fig. 4.15

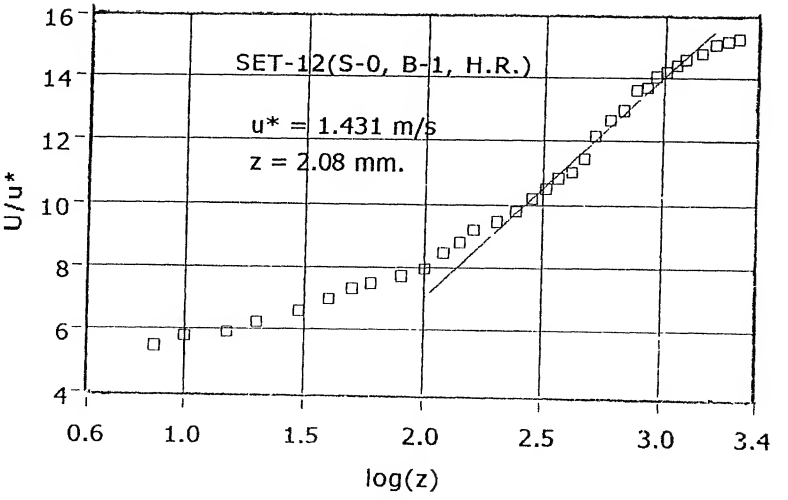

Fig 4.16

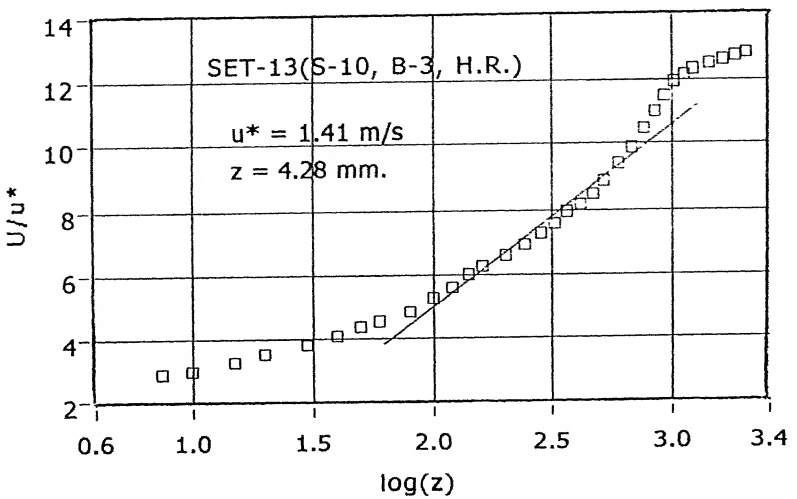

Fig. 4.17

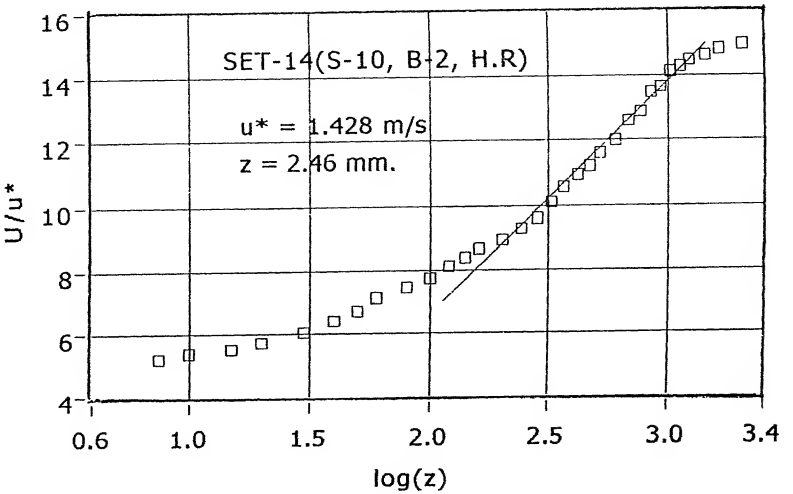

Fig. 4.18

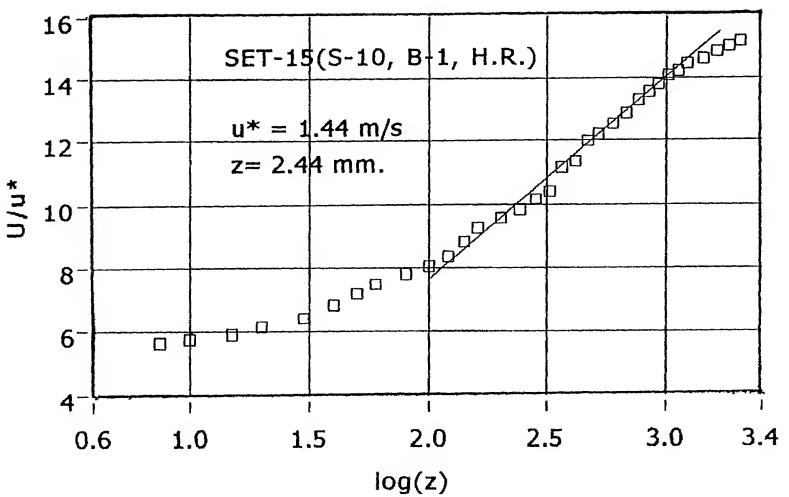

Fig. 4.19

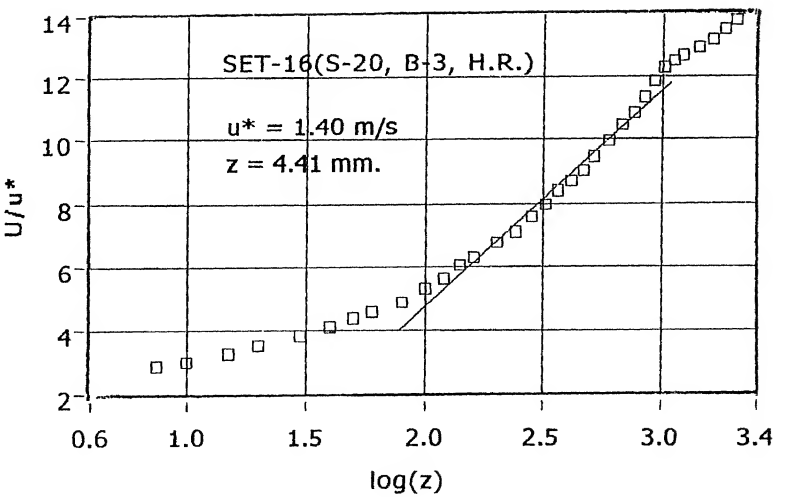

Fig. 4.20

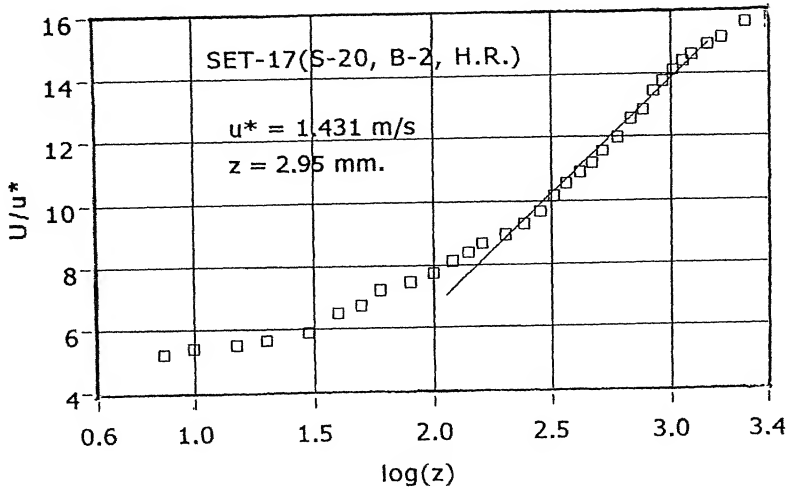

Fig. 4.21

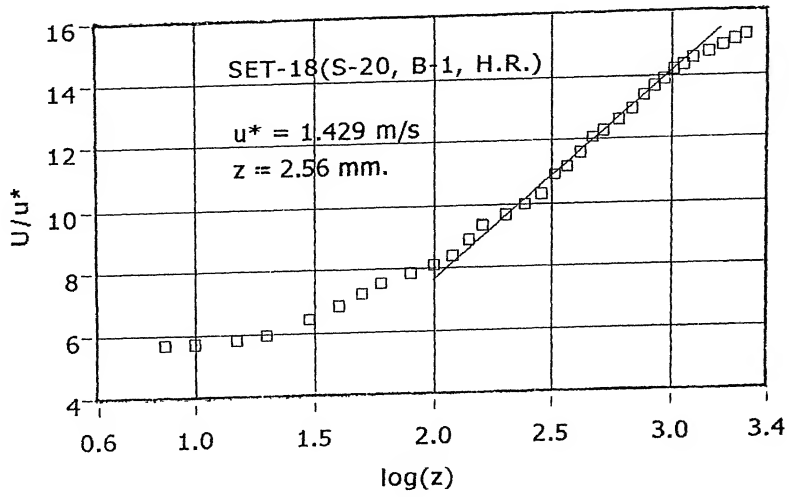

Fig. 4.22

Configura-Tion No.	Lower Velocity Profile $1/\alpha$	Upper Velocity Profile $1/\alpha$
1.	0.134	0.305
2.	0.130	0.281
3.	0.128	0.258
4.	0.131	0.290
5.	0.123	0.263
6.	0.122	0.241
7.	0.128	0.281
8.	0.120	0.253
9.	0.120	0.234
10.	0.126	0.290
11.	0.120	0.250
12.	0.120	0.240
13.	0.124	0.290
14.	0.120	0.254
15.	0.120	0.243
16.	0.125	0.278
17.	0.117	0.248
18.	0.120	0.238

Table 4.3: Power-Law Exponent for Lower and Upper Velocity Profiles

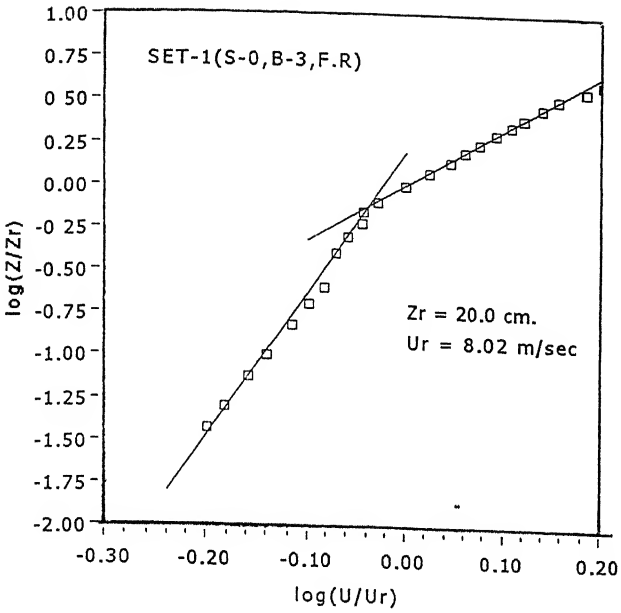

Fig. 4.23

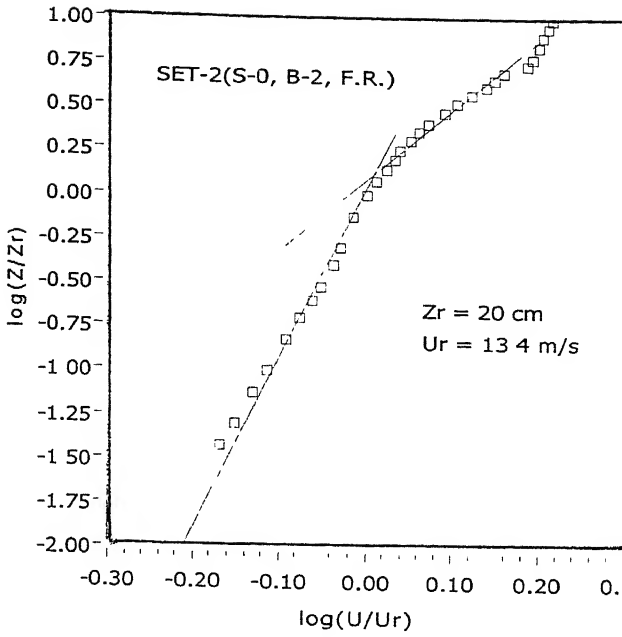

Fig. 4.24

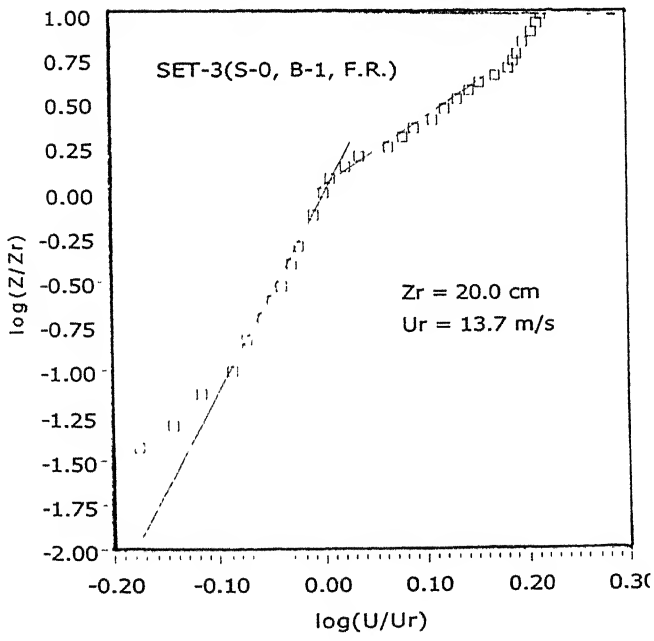

Fig. 4.25

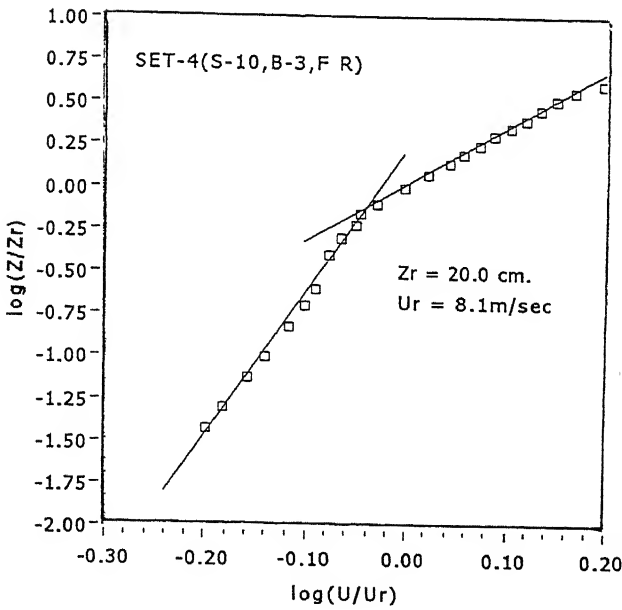

Fig. 4.26

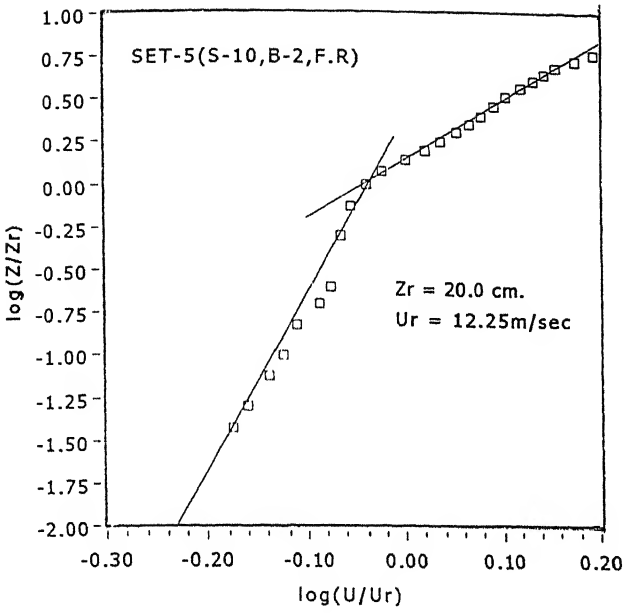

Fig 4.27

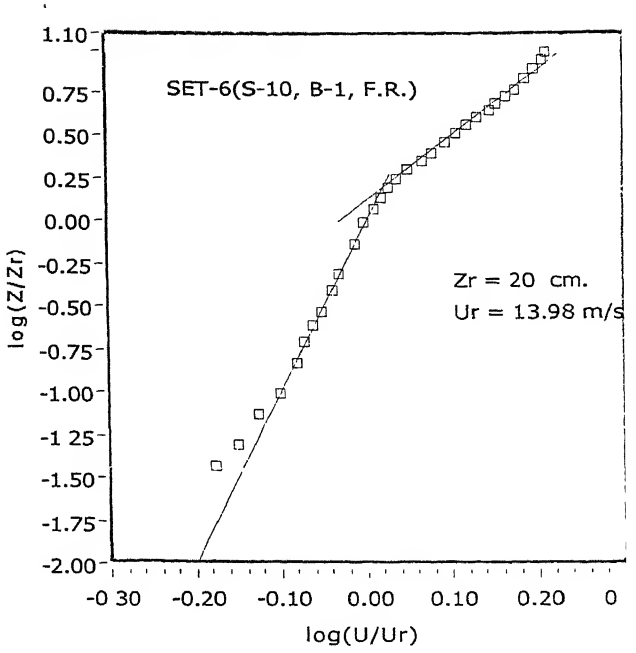

Fig. 4.28

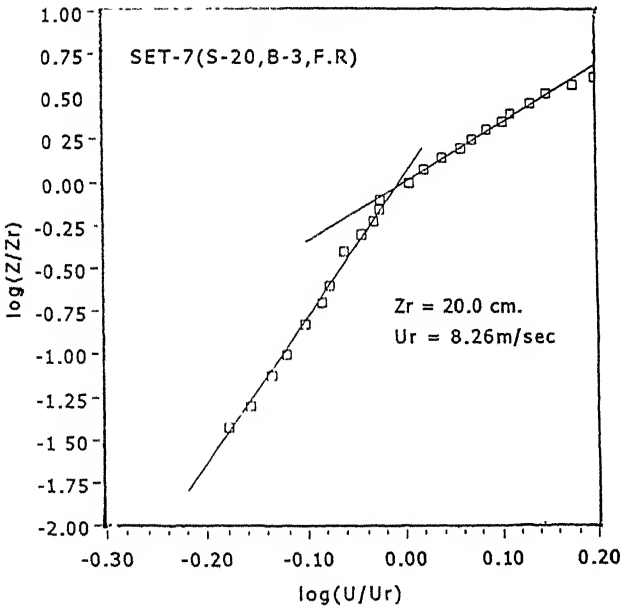

Fig. 4.29

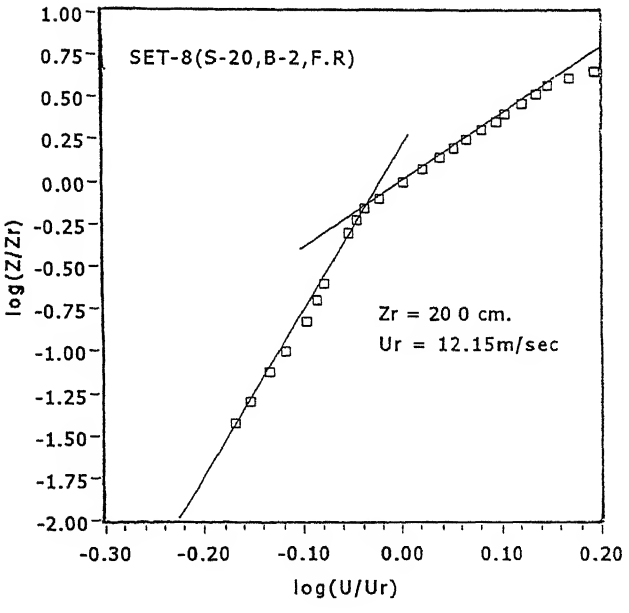

Fig. 4.30

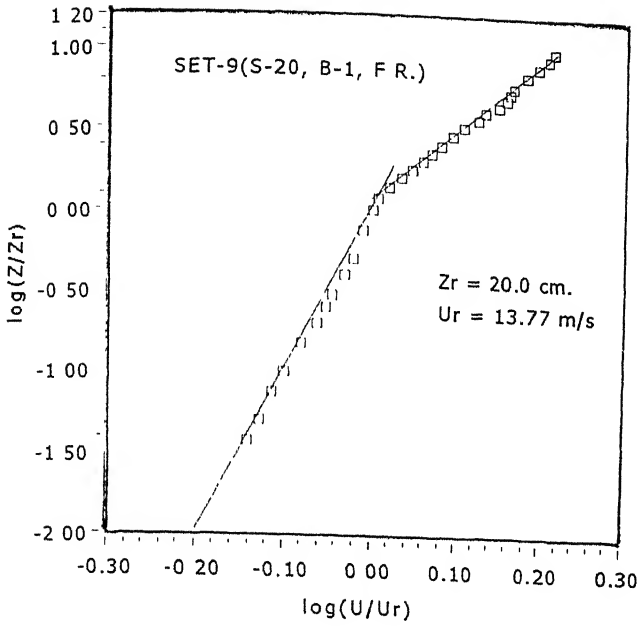

Fig. 4.31

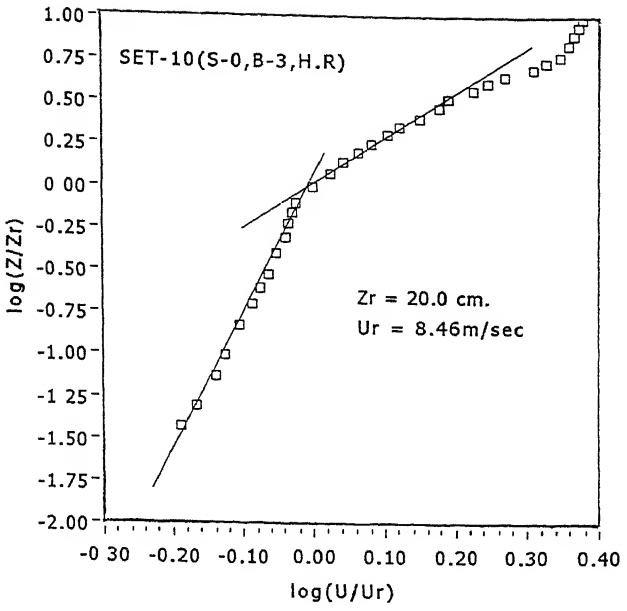

Fig. 4.32

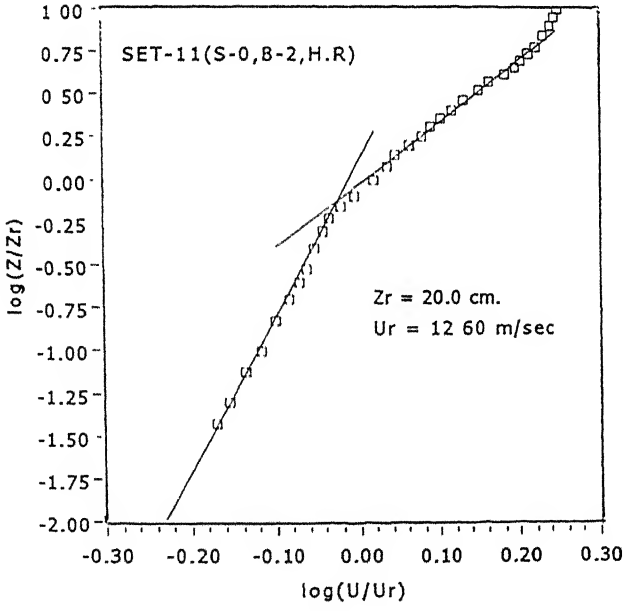

Fig. 4.33

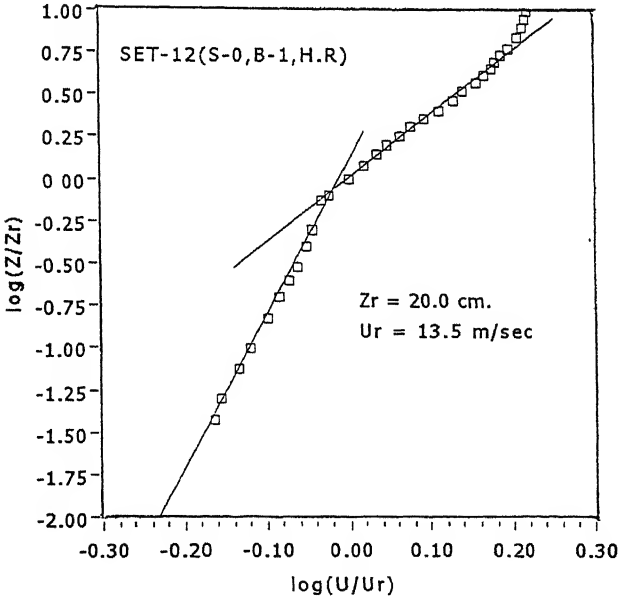

Fig. 4.34

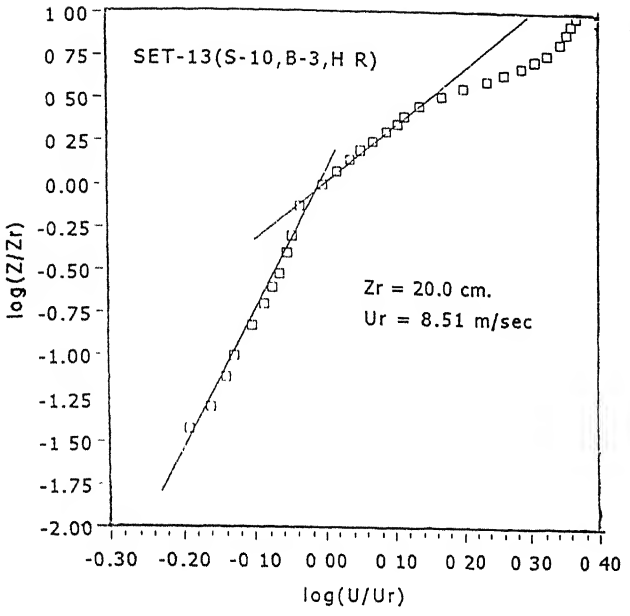

Fig 4.35

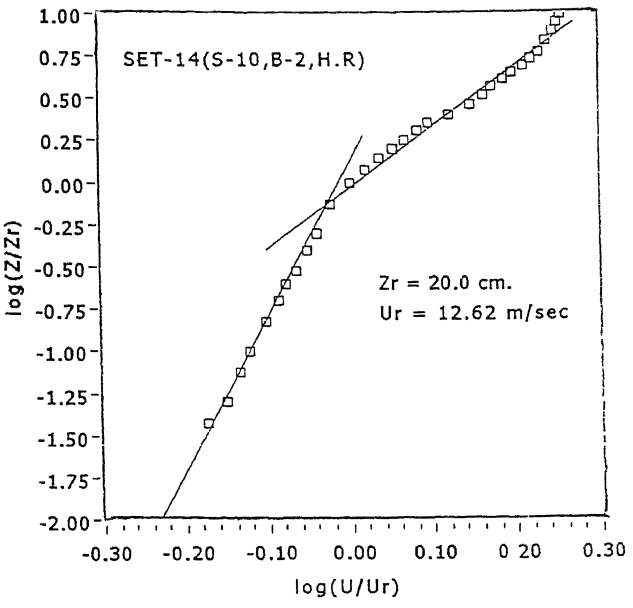

Fig 4.36

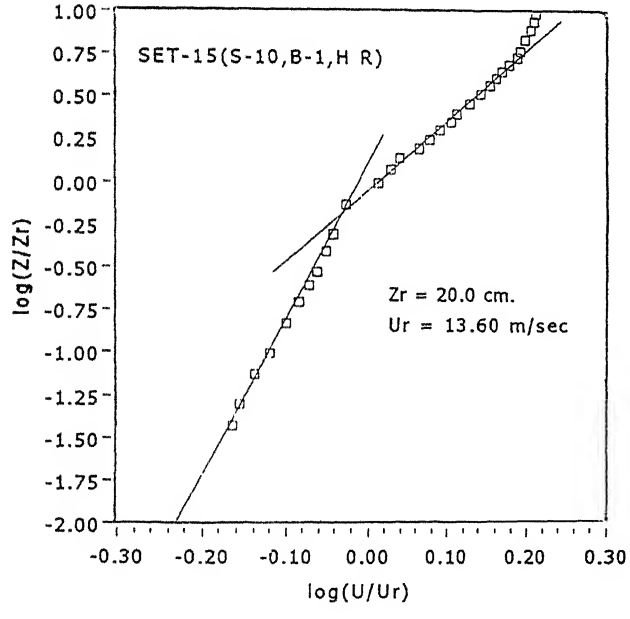

Fig. 4 37

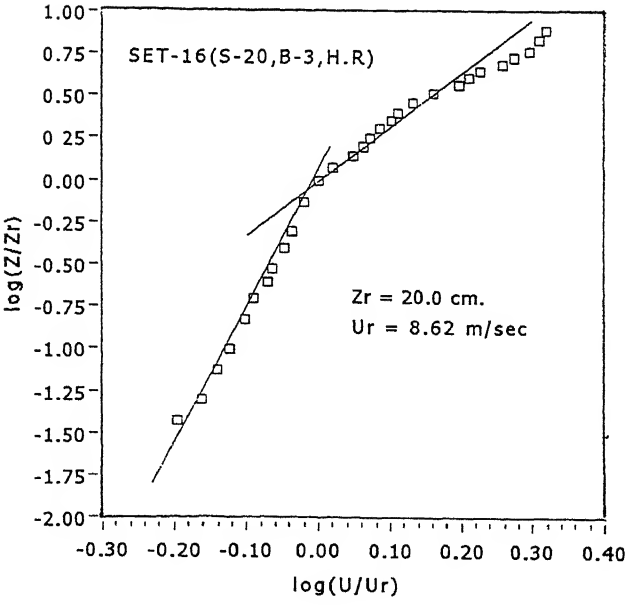

Fig. 4.38

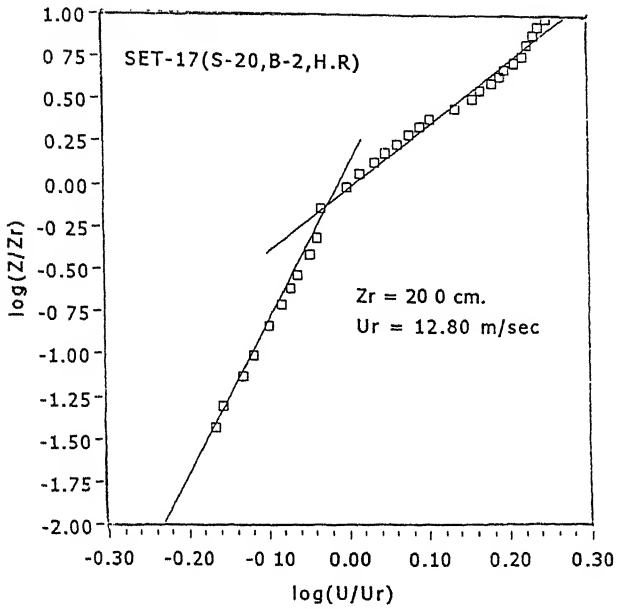

Fig 4 39

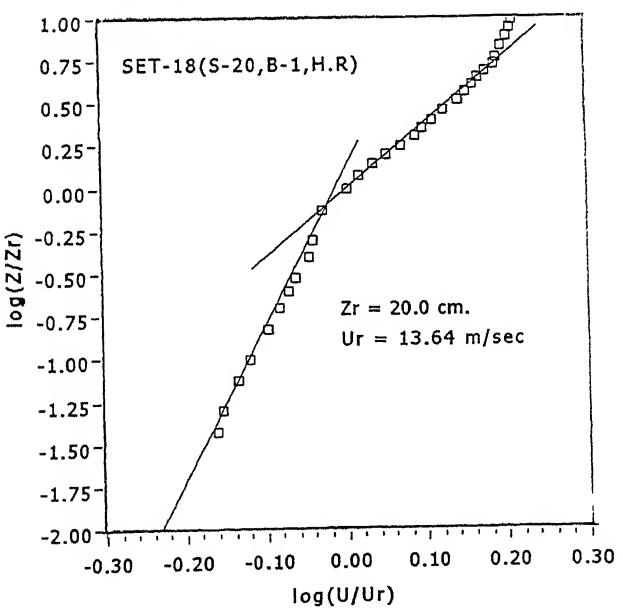

Fig. 4.40

Slot also has the same effect, helping in proper distribution of momentum deficit across the thickness of the boundary layer. For configurations 1-9 with full surface roughness, the value of exponent is larger in the upper regions than for corresponding lower regions.

Slot marginally changes the value of the exponent, both in upper and lower regions. In configurations where full barrier height was used, the value of power-law exponent is found slightly larger than that of the other two heights. Exponent is very large in the upper regions when the mixing devices are indispensable in that, they distribute the momentum deficit properly in the boundary layer thickness.

Figures 4.41-4.58 show the variation of turbulence intensity with the wind tunnel height, z. Exaggerated surface roughness is manifested in terms of local increase in turbulence intensities near the wall. The intensity falls with tunnel height, z. Slot, barrier and spires help to increase the turbulence intensities. The values in the curves compare well with the full-scale values reported by Tieleman [2] given in Fig. 4.59 .

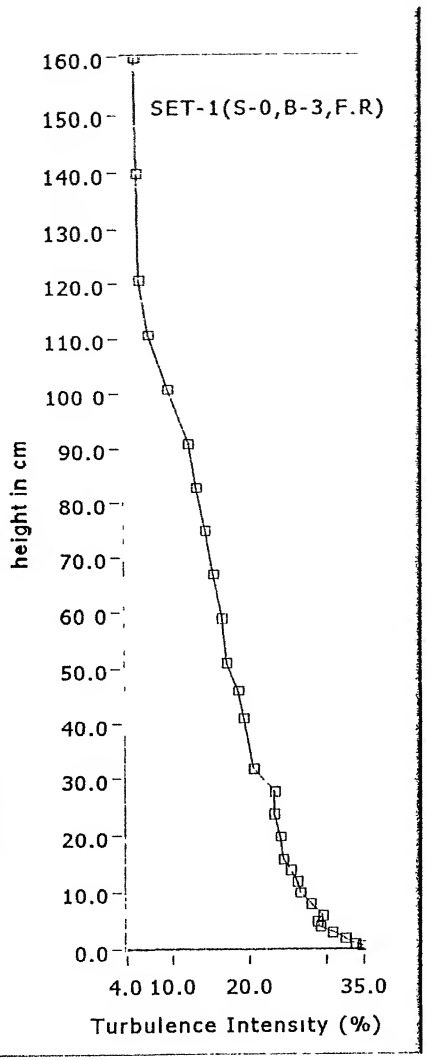

Fig 4.41

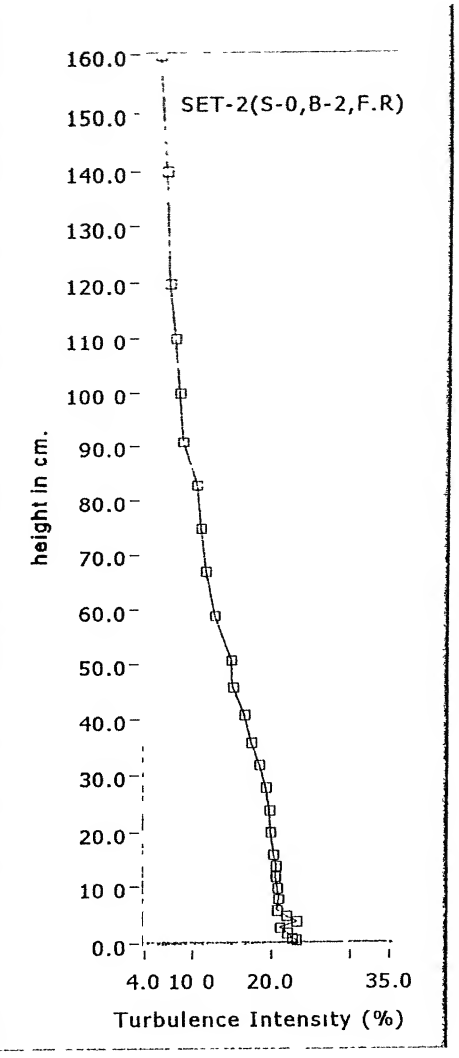

Fig. 4.42

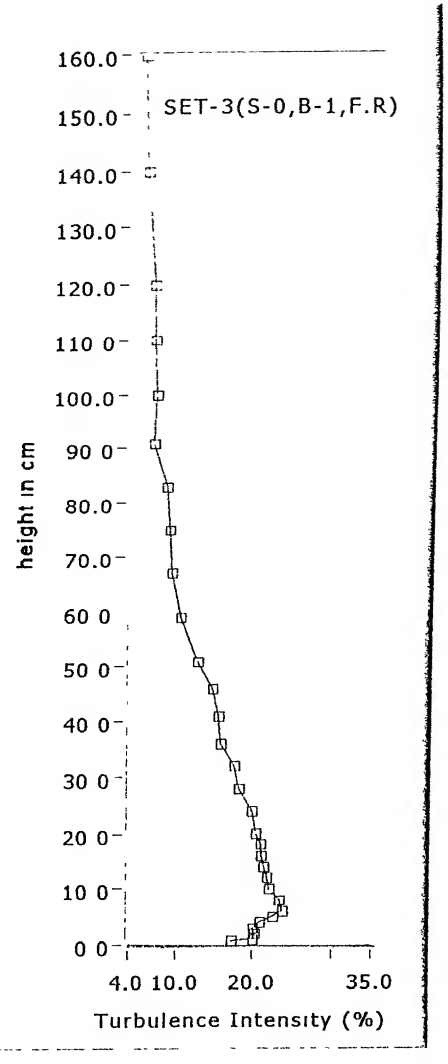

Fig. 4.43

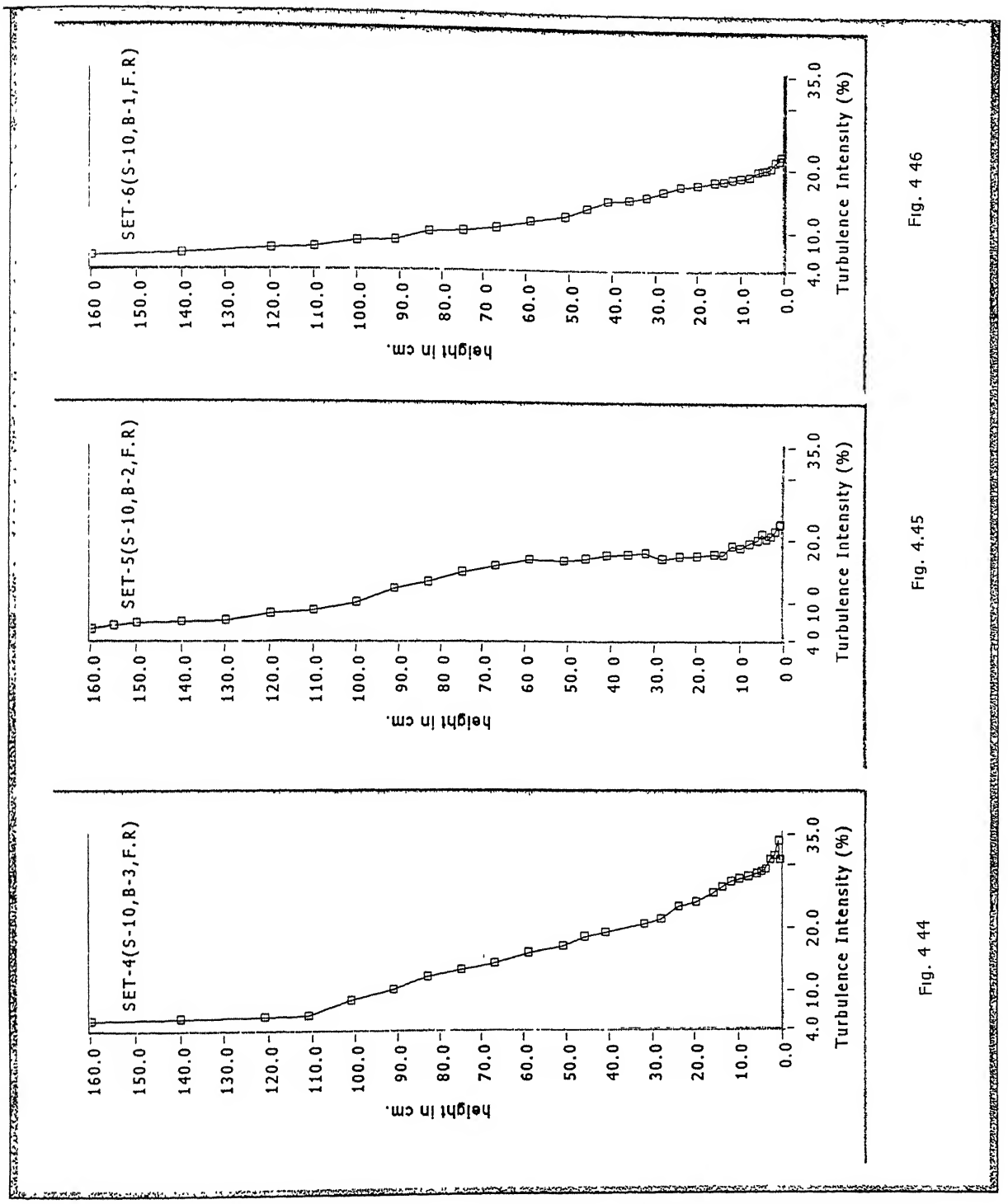

Fig. 4 44

Fig. 4.45

Fig. 4 46

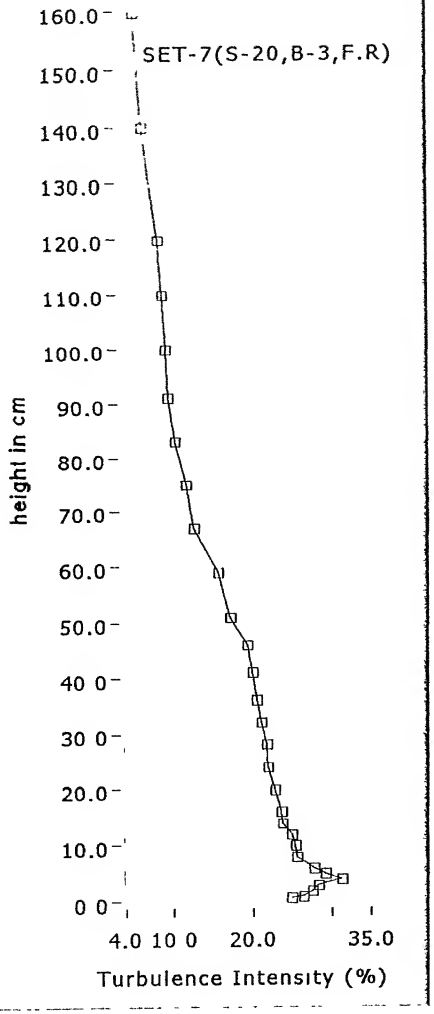

Fig 4.47

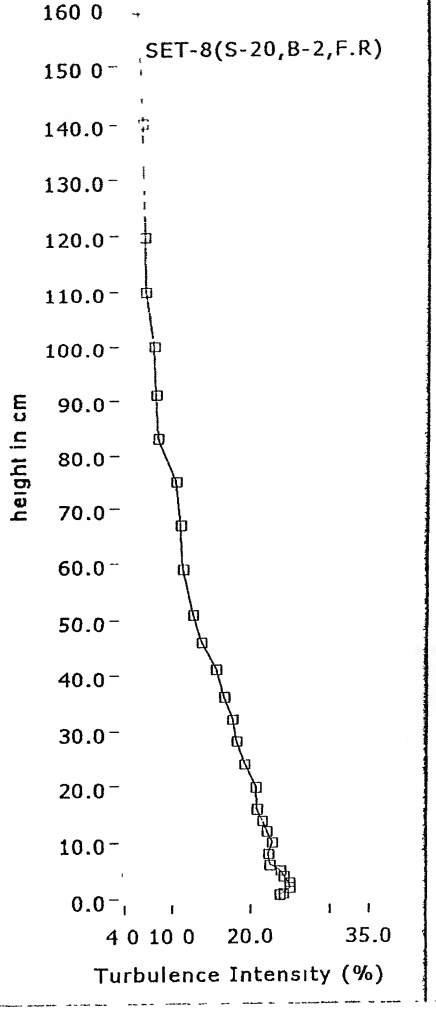

Fig 4.48

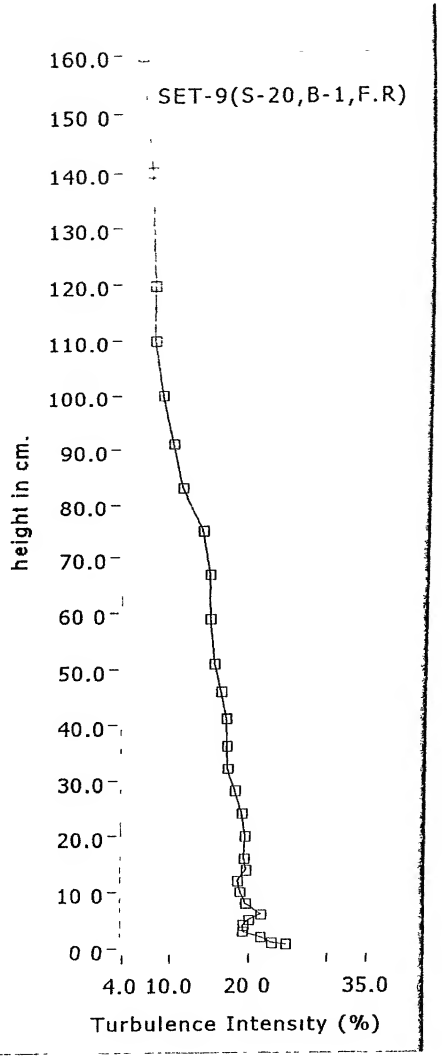

Fig. 4 49

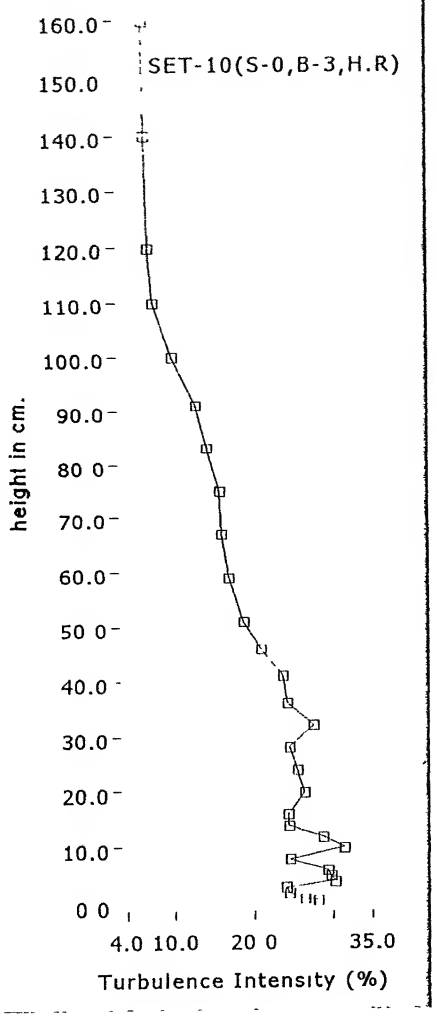

Fig. 4.50

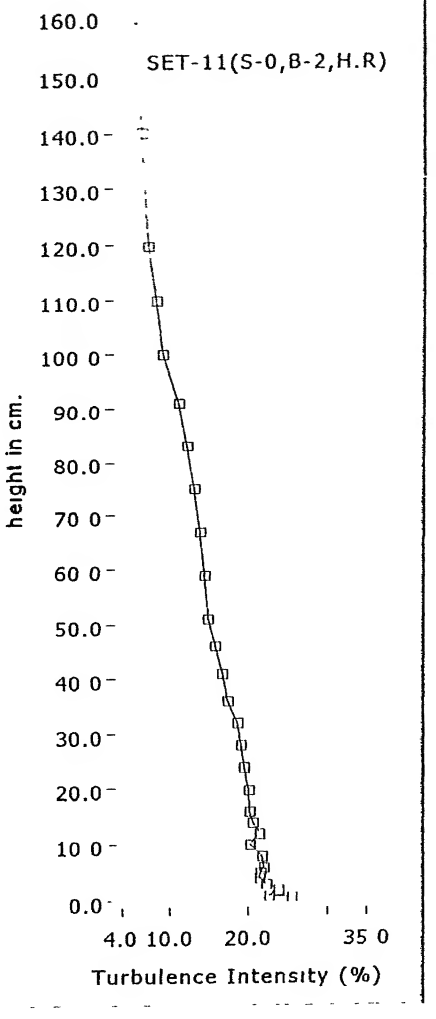

Fig 4.51

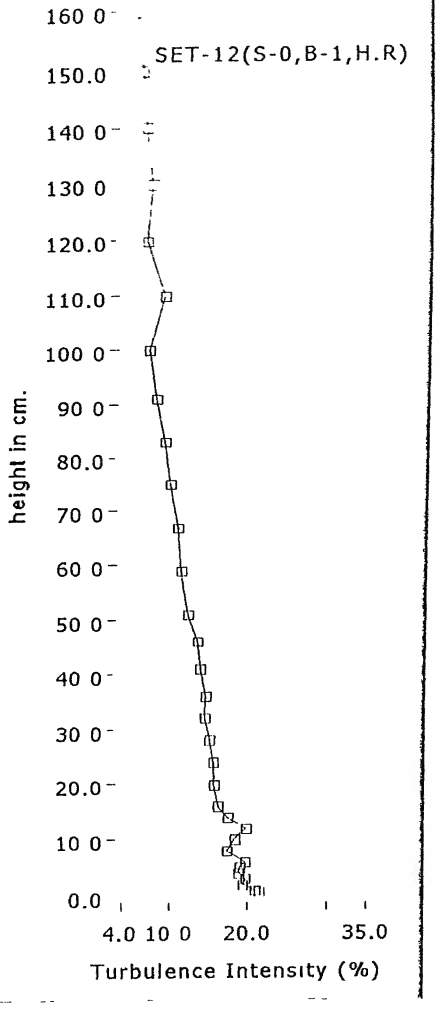

Fig. 4.52

Fig. 4.53

Fig. 4.54

Fig 4 55

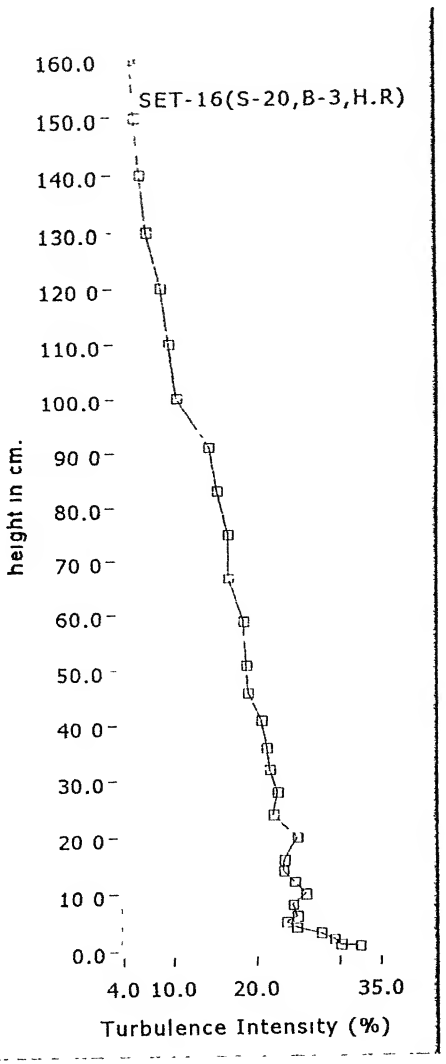

Fig. 4.56

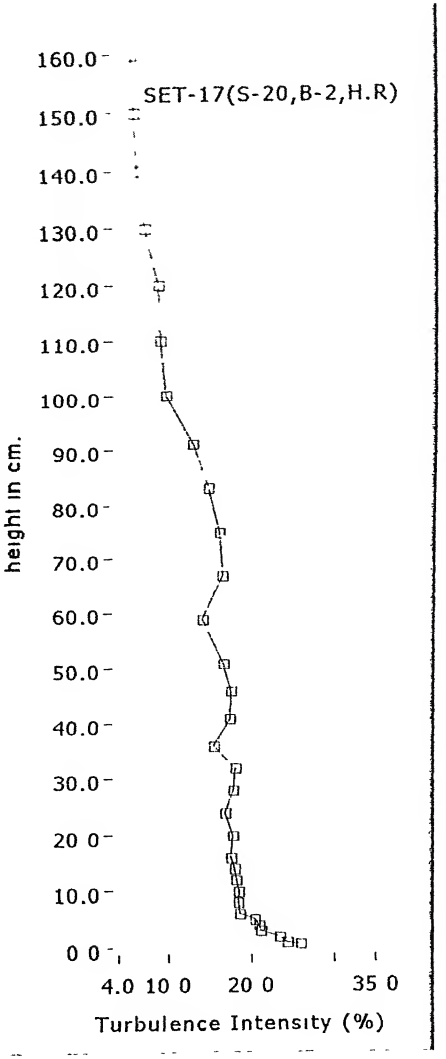

Fig. 4.57

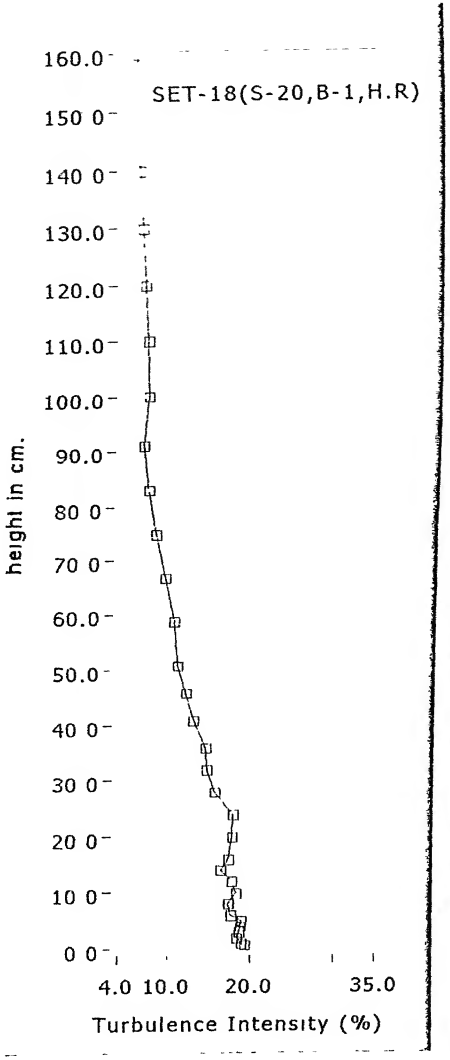

Fig. 4.58

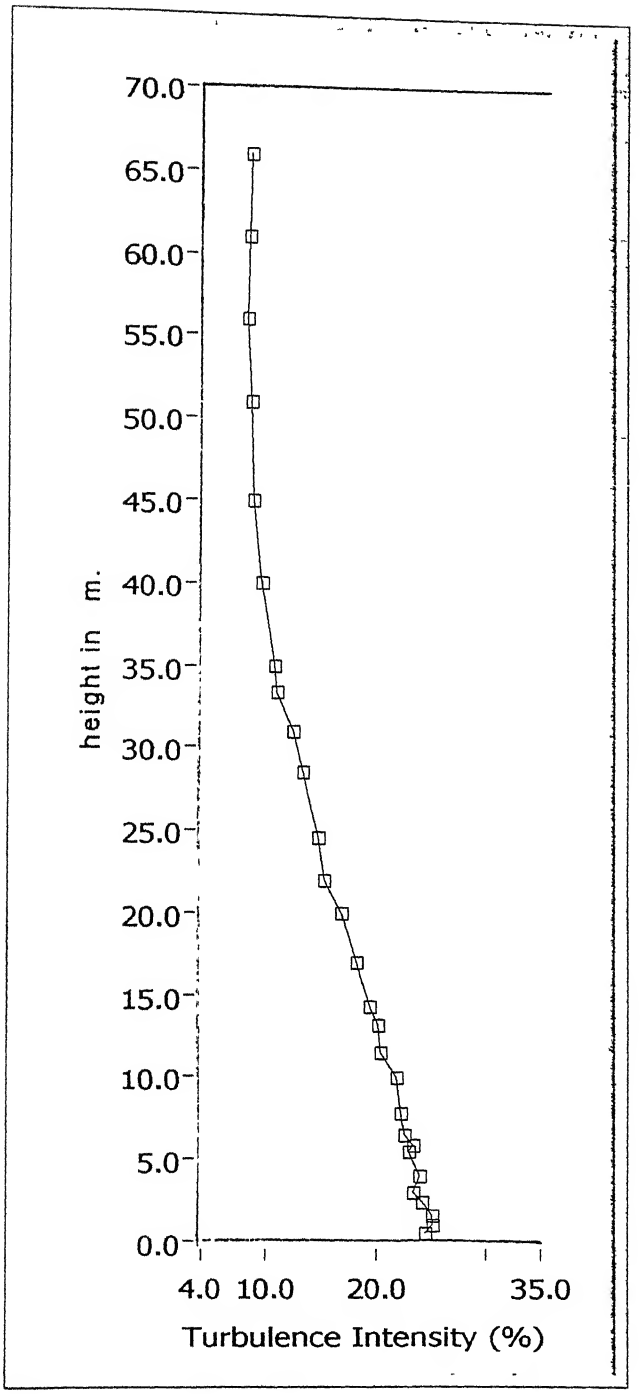

Fig. 4.59

(From Tieleman et. al. [2])

4.2 Atmospheric Longitudinal Length Scales of Turbulence Component

As mentioned before, the aeroelastic behavior of the structures in atmospheric boundary layer can be predicted by scaled-model experiments in the wind tunnels even when Reynolds number do not match, provided the scale factor for the longitudinal length-scale of turbulence, Lu_x, matches closely with the actual physical model-scale. The longitudinal length-scales for turbulence were calculated at different heights. Figure 4.60-4.77 show the longitudinal integral length scale with different heights for all configurations.

4.3 Model Scale Factors

Several procedures can be used to get the model scale factor. Proper model scale factor is necessary for good results. Some procedures are given below to deduce model scale factor.

1. Simulated boundary layer thickness.
2. Longitudinal length scale of streamwise component of turbulence.
3. By matching the aerodynamic roughness length of simulated model boundary layer and corresponding atmospheric boundary layer.

Of these two second procedure gives the best simulation of aeroelastic effects.

4.4 Determination of the Model Scale Factor Based on Longitudinal Length Scale of Turbulence

Using the procedure proposed by Cook [10], we first select a point in the boundary layer where the longitudinal length scale as measured above was maximum. This was quite uniformly at a height of 40 cm. in the wind tunnel.

At this height, we start with the model values of $(z)_M$, $(z_0)_M$ and $(Lu_x)_M$ with M denoting model, we assume a trial scale factor S_0=400, and with this value, we calculate the corresponding full-scale values of $(z)_F$, $(z_0)_F$ and $(Lu_x)_F$ with F denoting full scale. We next obtain the value of the longitudinal length scale of turbulence $(Lu_x)_a$ with a denoting atmosphere, for atmospheric data at this prototype value of z using the data of Fig. 4. The value of $(Lu_x)_a/(Lu_x)_M$ gives a corrected value of the scale factor S_1. We could iterate again to get convergence.

Data of Fig. 5 is also fitted to a curve to get a deterministic approach. E.S.D.U. [4] suggests an empirical formula for determining the scale factor.

$$S = \frac{91.3(z)_M^{0.491}}{(Lu_x)_M^{1.403}(z_0)_M^{0.088}} \tag{4.5}$$

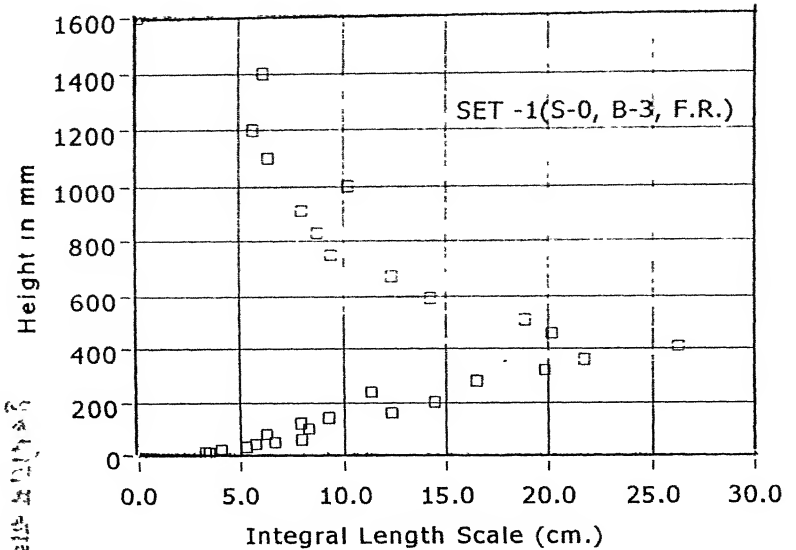

Fig. 4.60

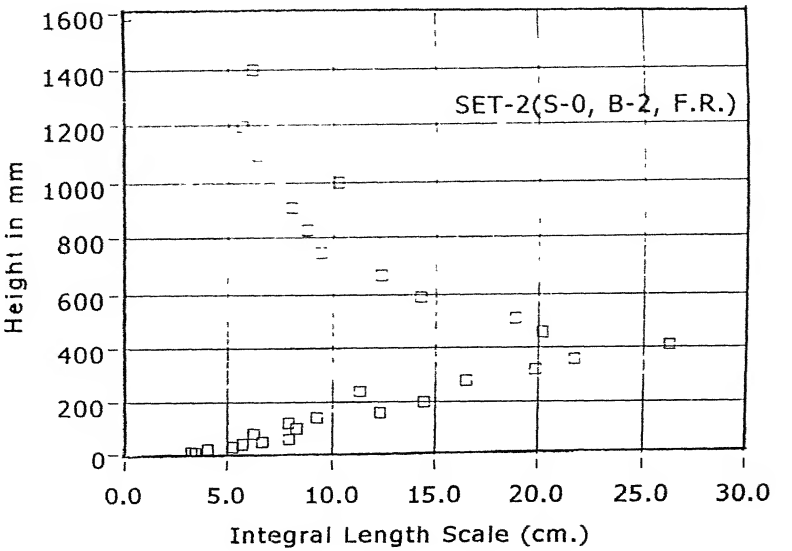

Fig. 4.61

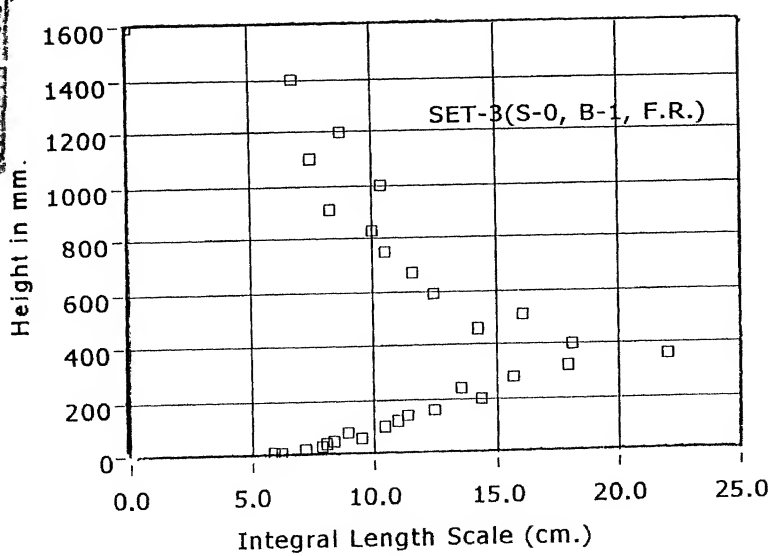

Fig. 4.62

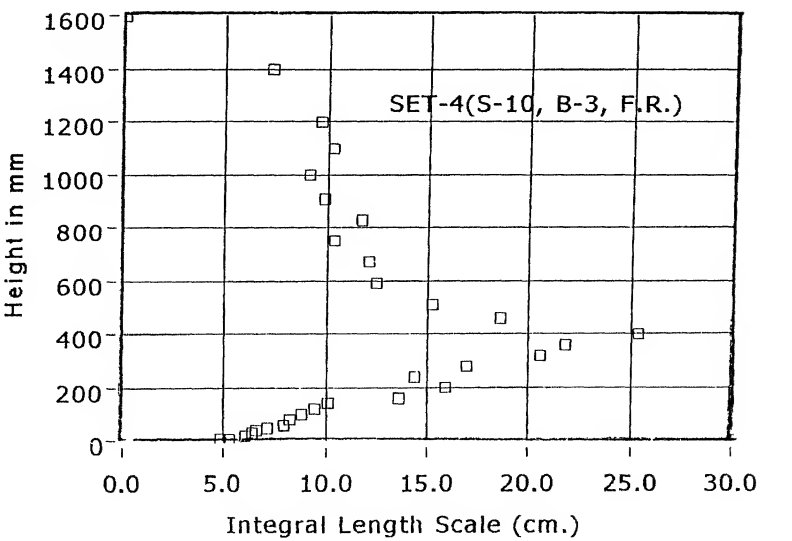

Fig. 4.63

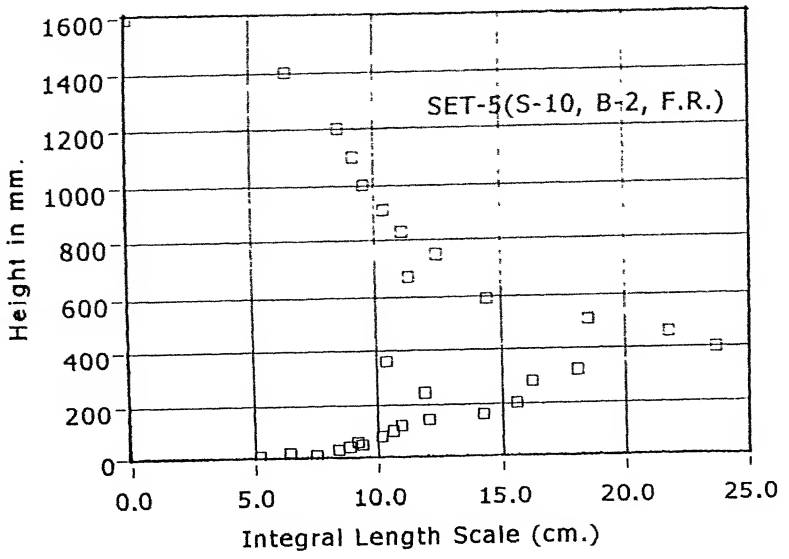

Fig. 4.64

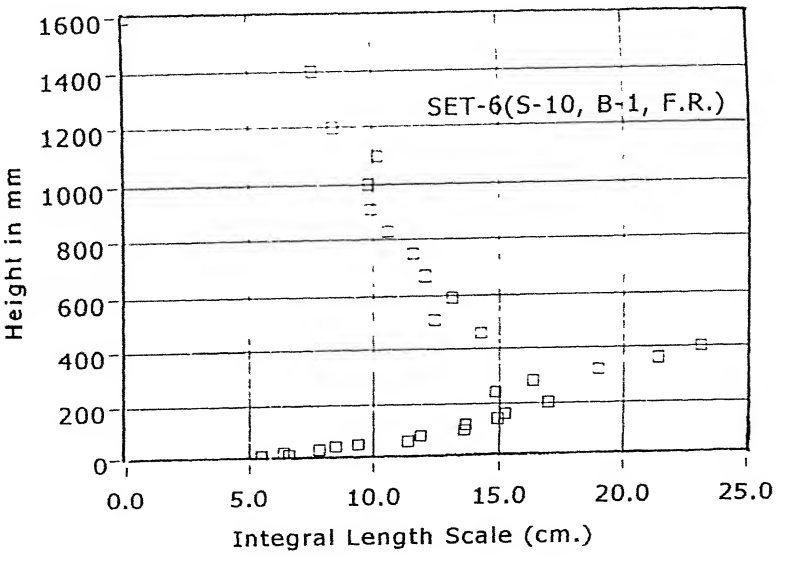

Fig. 4.65

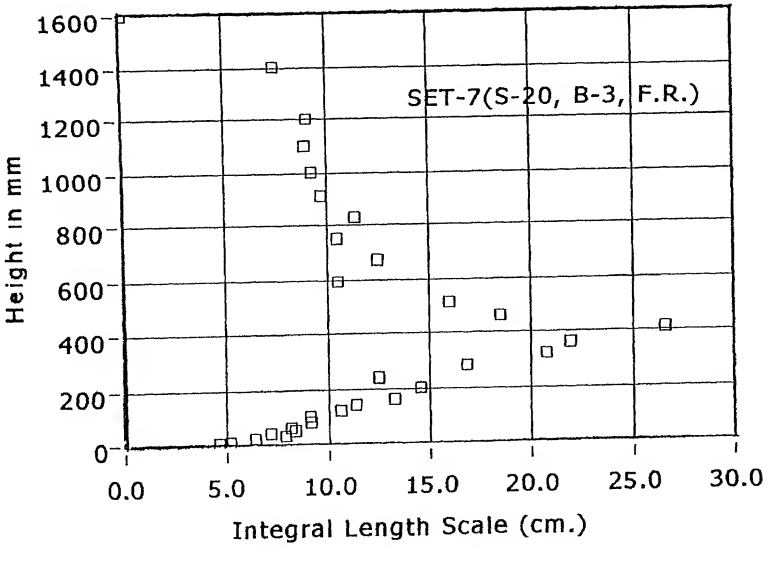

Fig. 4.66

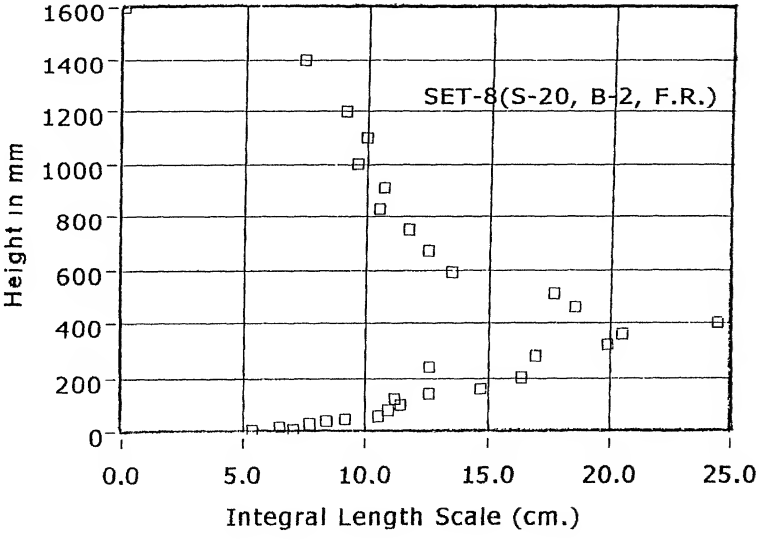

Fig. 4.67

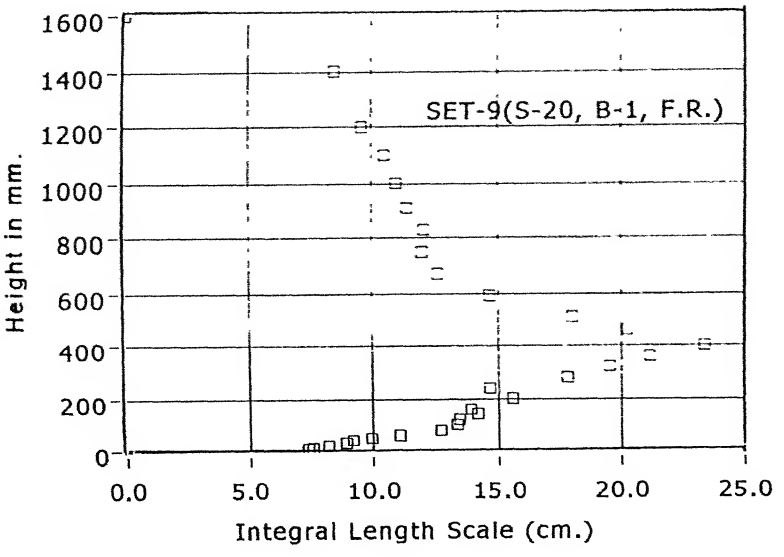

Fig. 4.68

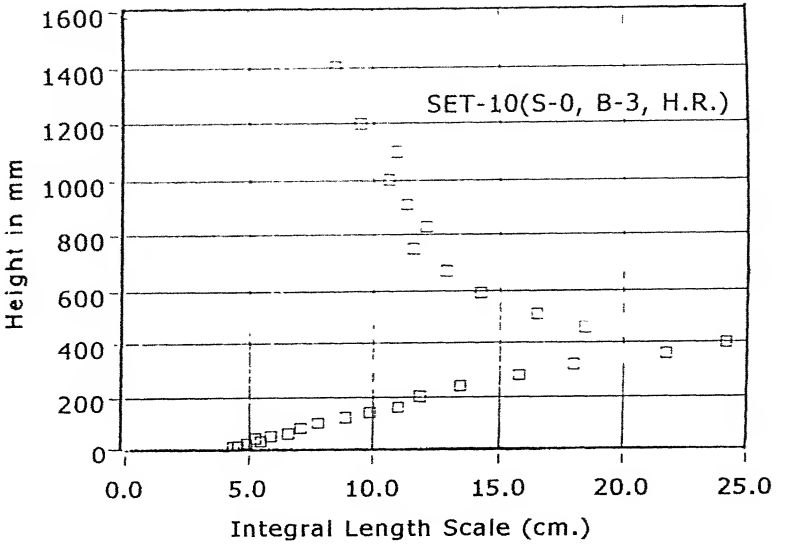

Fig. 4.69

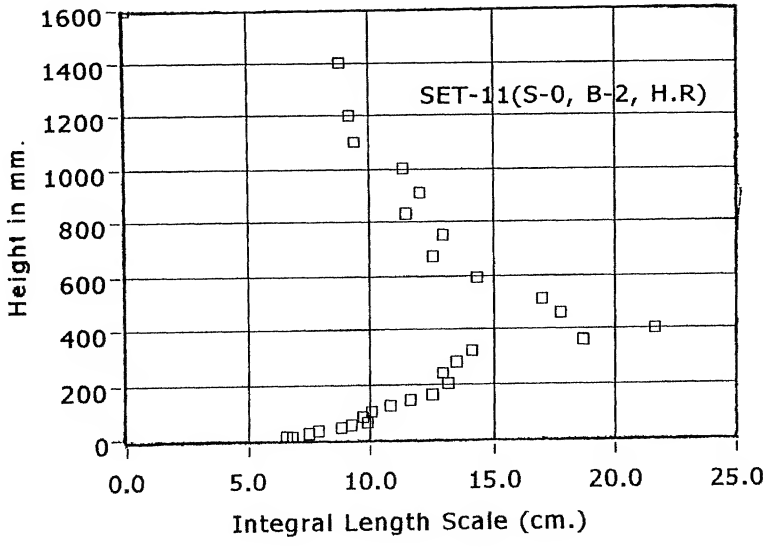

Fig. 4.70

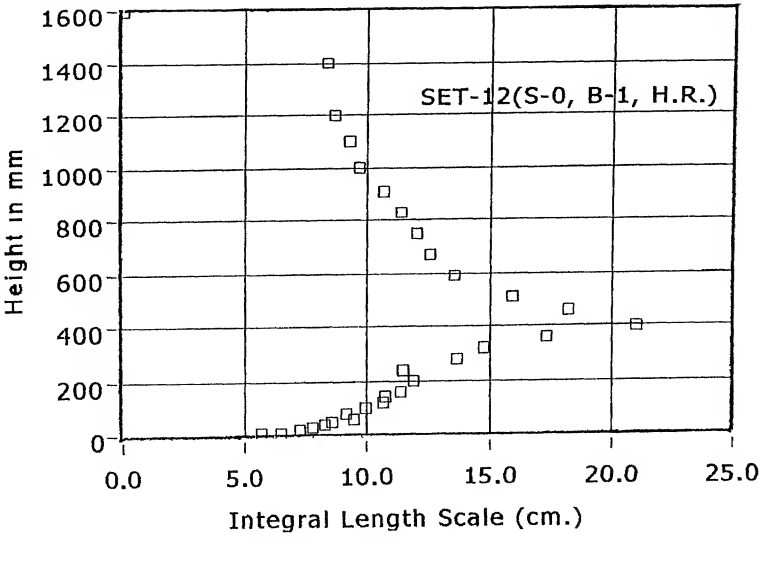

Fig. 4.71

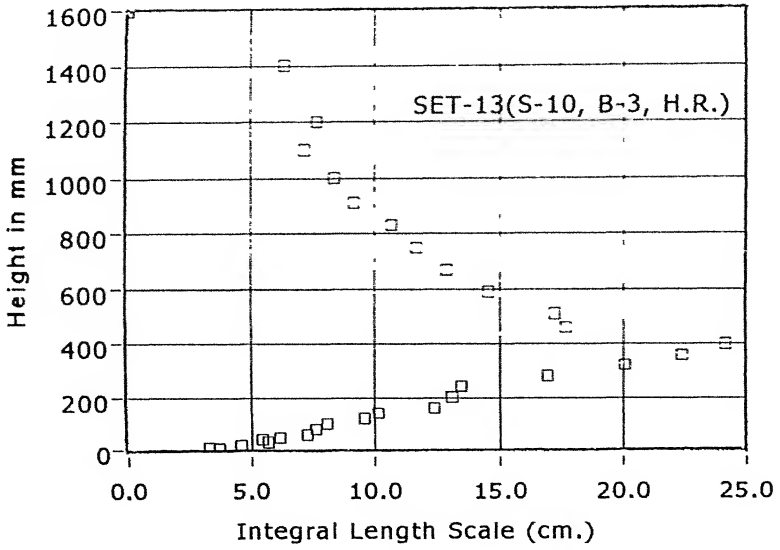

Fig. 4.72

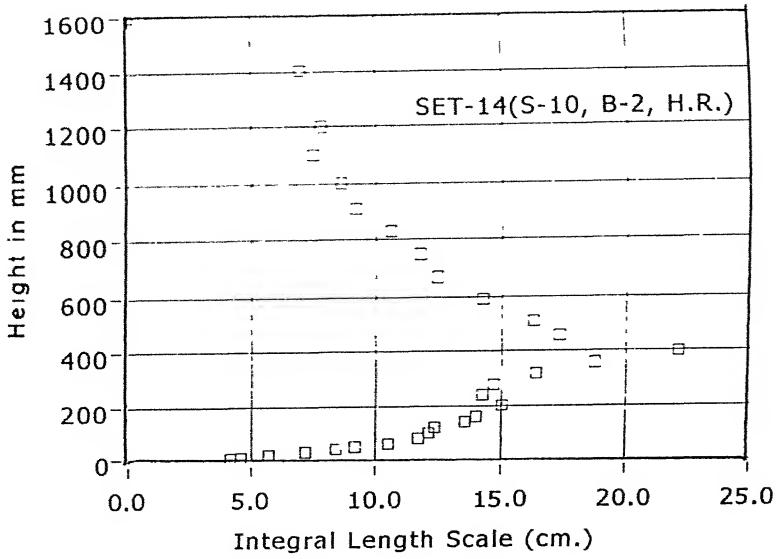

Fig. 4.73

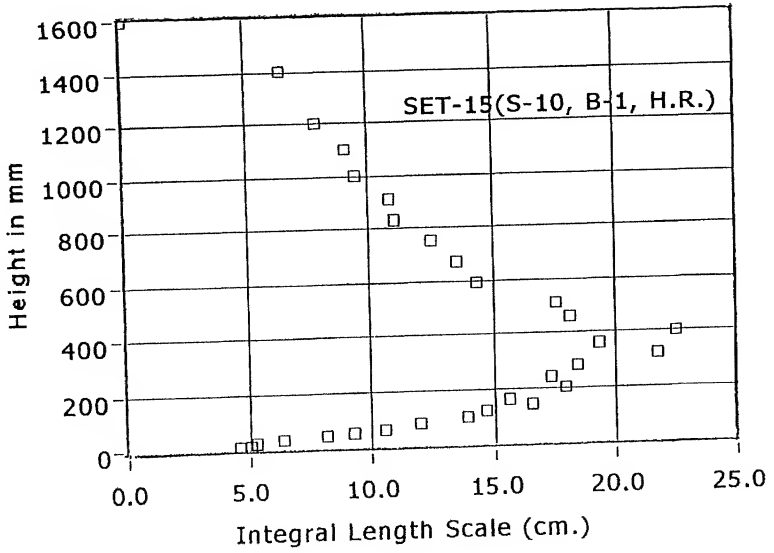

Fig. 4.74

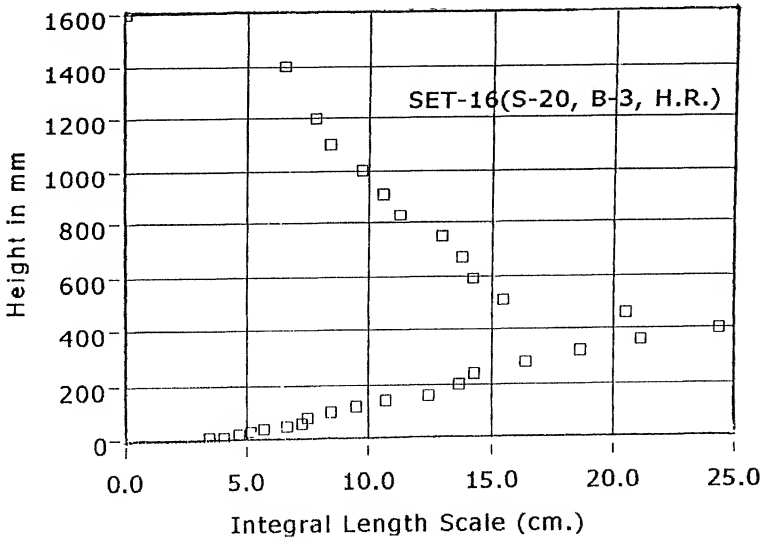

Fig. 4.75

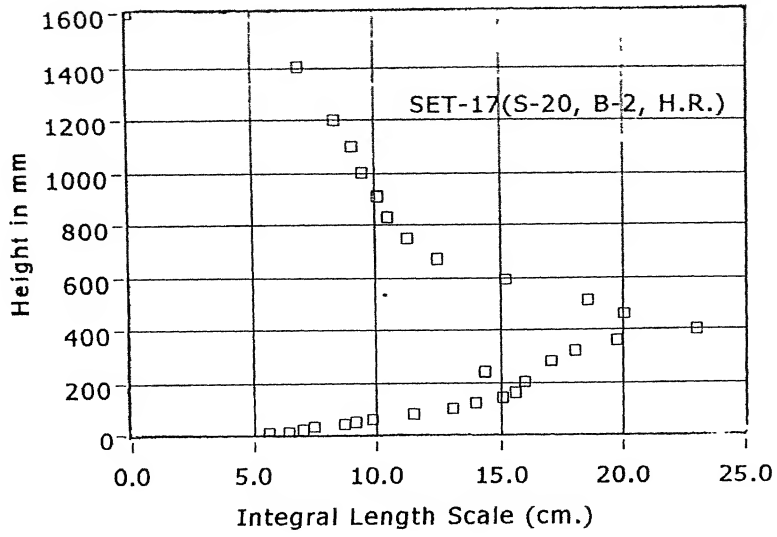

Fig. 4.76

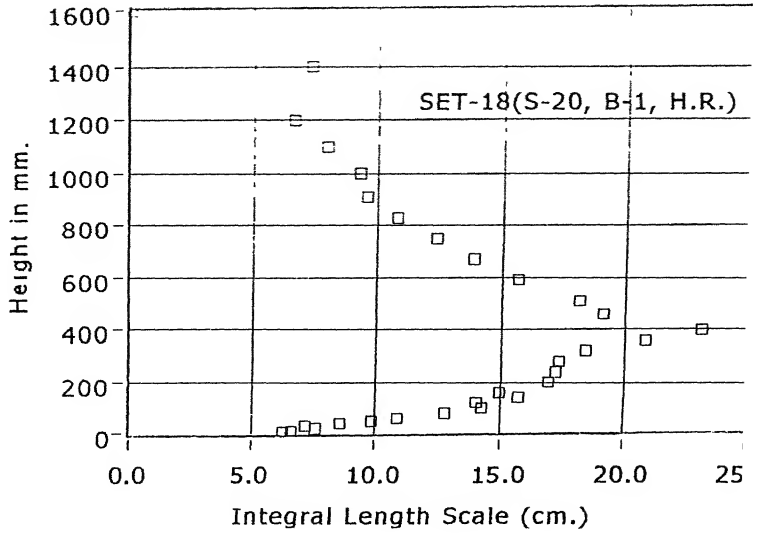

Fig. 4.77

This is a little simpler procedure and gives almost the same value at the iterative preocedure. Table 4.4 gives the model scale factors calculated from the measured data for all the configurations.

Table 4.5-4.13 show the matching of simulated integral length scale with natural length scale in atmospheric boundary layer for all configurations.

S.No.	u*(U.P) m/sec	z_0(U.P) mm	S.F.(U.P)
1.	1.451	6.38	617
2.	1.553	4.68	713
3.	1.548	3.84	759
4.	1.462	6.51	605
5.	1.563	4.91	681
6.	1.568	4.12	743
7.	1.474	6.91	565
8.	1.601	5.18	652
9.	1.611	4.72	712
10.	1.406	4.116	685
11.	1.421	2.37	829
12.	1.431	2.08	868
13.	1.461	4.28	673
14.	1.428	2.46	792
15.	1.44	2.44	812
16.	1.400	4.41	666
17.	1.431	2.95	744
18.	1.429	2.56	782

Table 4.4: Calculation for Model Scale Factor

z (M) cm.	Configuration 1			Configuration 2		
	z (F) m	Lu_x (F) m	Lu_x (ABL)	z (F) m	Lu_x (F) m	Lu_x (ABL)
5	30.8	41	85	35.6	55	99
10	61.7	51	104	71.3	64	121
15	92.5	57	121	107.0	81	150
20	123.4	89	142	142.6	104	182
30	185.1	122	191	213.9	138	209
40	246.8	161	218	285.2	166	218
50	308.5	126	211	356.5	106	148

Table 4.5: Matching of Simulated Integral Length Scale with Natural Length Scale in Atmospheric Boundary Layer for Configurations 1 and 2.

z (M) cm.	Configuration 3			Configuration 4		
	z (F) m	Lu_x (F) m	Lu_x (ABL)	z (F) m	Lu_x (F) m	Lu_x (ABL)
5	38.0	63	102	30.2	43	82
10	75.9	79	117	60.5	53	106
15	113.9	86	144	90.75	61	120
20	151.8	107	181	121.0	96	142
30	227.7	136	216	181.5	124	196
40	303.6	163	203	242.0	152	219
50	379.5	122	161	302.5	92	201

Table 4.6: Matching of Simulated Integral Length Scale with Natural Length Scale in Atmospheric Boundary Layer for Configurations 3 and 4.

z (M) cm.	Configuration 7			Configuration 8		
	z (F) m	Lu_x (F) m	Lu_x (ABL)	z (F) m	Lu_x (F) m	Lu_x (ABL)
5	28.2	47	78	32.6	71	102
10	56.5	51	104	65.2	78	116
15	85.0	64	115	98.0	86	138
20	113.0	82	140	130.4	112	175
30	169.5	117	193	195.6	136	216
40	226.0	149	222	260.8	167	222
50	282.5	90	190	326.0	121	172

Table 4.8: Matching of Simulated Integral Length Scale with Natural Length Scale in Atmospheric Boundary Layer for Configurations 7 and 8.

z (M) cm.	Configuration 9			Configuration 10		
	z (F) m	Lu_x (F) m	Lu_x (ABL)	z (F) m	Lu_x (F) m	Lu_x (ABL)
5	35.6	88	105	34.2	40	104
10	71.2	95	117	68.5	53	121
15	107.0	101	144	102.8	67	144
20	142.4	111	181	137.0	81	191
30	213.6	139	216	205.5	123	211
40	284.8	175	203	274.0	171	209
50	356.0	128	161	342.5	113	164

Table 4.9: Matching of Simulated Integral Length Scale with Natural Length Scale in Atmospheric Boundary Layer for Configurations 9 and 10.

z (M) cm.	Configuration 11			Configuration 12		
	z (F) m	Lu_x (F) m	Lu_x (ABL)	z (F) m	Lu_x (F) m	Lu_x (ABL)
5	41.4	76	107	43.4	84	109
10	82.9	83	128	86.8	86	126
15	124.4	96	168	130.2	93	160
20	165.8	109	211	173.6	103	202
30	248.8	117	216	260.4	128	208
40	331.6	164	174	347.2	161	158
50	414.5	141	157	434.0	106	140

Table 4.10: Matching of Simulated Integral Length Scale with Natural Length Scale in Atmospheric Boundary Layer for Configurations 11 and 12.

z (M) cm.	Configuration 13			Configuration 14		
	z (F) m	Lu_x (F) m	Lu_x (ABL)	z (F) m	Lu_x (F) m	Lu_x (ABL)
5	33.6	41	97	39.6	73	106
10	67.3	54	119	79.2	110	123
15	101.0	68	141	118.8	131	152
20	134.6	88	190	158.4	152	200
30	202	135	208	237.6	172	221
40	269.2	158	210	316.8	178	182
50	336.5	116	165	396.0	139	163

Table 4.11: Matching of Simulated Integral Length Scale with Natural Length Scale in Atmospheric Boundary Layer for Configurations 13 and 14.

z (M) cm.	Configuration 15			Configuration 16		
	z (F) m	Lu_x (F) m	Lu_x (ABL)	z (F) m	Lu_x (F) m	Lu_x (ABL)
5	40.6	74	110	33.3	44	96
10	81.2	98	126	66.6	56	116
15	121.8	110	145	99.9	71	131
20	162.4	122	206	133.2	91	168
30	243.6	133	218	199.8	124	201
40	343.6	178	176	266.4	162	210
50	406.0	132	160	333.0	103	171

Table 4.12: Matching of Simulated Integral Length Scale with Natural Length Scale in Atmospheric Boundary Layer for Configurations 15 and 16.

z (M) cm.	Configuration 17			Configuration 18		
	z (F) m	Lu_x (F) m	Lu_x (ABL)	z (F) m	Lu_x (F) m	Lu_x (ABL)
5	37.2	73	111	39.1	71	108
10	74.4	106	131	78.2	102	123
15	111.6	117	172	117.3	118	162
20	148.8	126	209	156.4	125	201
30	223.2	137	224	234.6	141	209
40	297.6	172	201	312.8	174	188
50	372.0	135	176	391.0	145	148

Table 4.13: Matching of Simulated Integral Length Scale with Natural Length Scale in Atmospheric Boundary Layer for Configurations 17 and 18.

Chapter 5

Conclusions

Based on results presented in Tables- 4.5-4.13, it is very clear that the effective length-scale factor decreases as we increase a) The barrier height, b) The slot-width in the extension board into the contraction cone, and c) The roughness element distribution on the test-section floor. It is further seen that:

1. The slot in the extension board appears to contribute much to decrease the length scale.

2. The maximum length-scale factor is obtain in configuration no. 7, where 20 cm slot is used, 30 cm. of barrier is used, and full roughness elements are distributed on the entire length.

The minimum scale factor of 565 is really too high for much meaningful work,unless very tall structures on models of large geographical areas are being investigated. It would appear that we can reduce the effective scale factor by increasing the slot-width still further.

One method for decreasing the scale factor, which has been tried earlier, is the castellation of the barrier top [11]. This probably should be attempted in further investigation.

Bibliography

[1] M. R. Hajj, I. M. Janajreh and H. W. Tieleman," Analysis of the Relation Between Atmosperic Wind and Pressure Fluctuations on a Low-Rise Building with Orthonormal Wavelet, ", *Proceedings of the 2nd European and African Conference on Wind Engineering*, Genova, Italy, June 22-26, 1997.

[2] Tieleman, H.W. and A. R. Timothy (1978), " Wind tunnel simulation of atmospheric surface layer for the study of wind loads on low-rise buildings", *Journal of Industrial Aerodynamics*, Vol. 3, pp. 21-38.

[3] " Characteristics of wind speed in lower layers of atmospheric near the ground: strong winds (natural atmosphere)", *ESDU Data Item No. 72026, Engineering Science Data Unit*, London, 1972.

[4] " Characteristics of atmospheric turbulence near the ground", *ESDU Data Item No. 74030, 74031, Engineering science Data Unit*, London, 1974,1975.

[5] Counihan, J. (1975), " Adiabatic atmospheric boundary layers: A review and analysis of data from the period 1880-1972", *Atmospheric Environment*, Vol. 9, pp. 871-905.

[6] Devenport, A.G. and Isyumov, N. (1967), " The application of atmospheric boundary layer wind tunnel to the prediction of wind loading, wind effects on buildings and structures", Ottawa, Canada, *University of Toronto Press*, pp. 210-230.

[7] Pasquill F. (1967), " Wind structure in the atmospheric boundary layer", em Discuss on Archit Aero. Phill. Trans. R-Soc-A269, pp. 321-554.

[8] Gupta, V. and Yadav, D. (1987), " Aerodynamic Study of Chimneys", *High Speed Aerodynamics Laboratory TRI-97*, Department of Aerospace Engineering, Indian Institute of Technology, Kanpur.

[9] Perry, A.E. and Joubert, P.N. (1973), " Roughwall boundary layers in adverse pressure gradients", *Journal of Fluid Mechanics*, Vol. 17, pp. 193-221.

[10] Cook, N.J. (1978), " Determination of model-scale factor in wind-tunnel simulations of the adiabatic boundary layer", *Journal of Industrial Aerodynamics*, Vol. 2, pp. 311-321.

[11] Cook, N.J. (1978), " Wind-tunnel simulation of adiabatic atmospheric boundary layer by roughness, barrier and mixing device method", *Journal of Industrial Aerodynamics*, Vol. 3, pp. 157-176.